N° d'ordre : **ANNÉE 2014**

THÈSE / UNIVERSITÉ DE RENNES 1
sous le sceau de l'Université Européenne de Bretagne

pour le grade de

DOCTEUR DE L'UNIVERSITÉ DE RENNES 1

Mention : Biologie et Sciences de la Santé

Ecole doctorale : Vie-Agro-Santé

présentée par

Claire HAEGELEN

préparée à l'unité de recherche U1099 LTSI MediCIS
Modélisation des connaissances et procédures chirurgicales et interventionnelles
Composante universitaire : Sciences de la vie et de l'environnement

---

Construction et validation d'une base de données multimodales pour la stimulation cérébrale profonde

Thèse soutenue à Rennes le 8 avril 2014

devant le jury composé de :

Sophie COLNAT-COULBOIS
PUPH, CHU Nancy / *examinateur*

Stephan CHABARDES
PUPH, CHU Grenoble / *rapporteur*

Emmanuel CUNY
PUPH, CHU Bordeaux / *rapporteur*

Marc VERIN
PUPH, CHU Rennes / *examinateur*

Xavier MORANDI
PU-PH, CHU Rennes / *directeur de thèse*

Pierre JANNIN
CR1, Université Rennes I / *co-directeur de thèse*

Remerciements

A mon père,

Je dédie cette thèse à Emmanuel et à sa patience quotidienne qui a permis l'aboutissement de ce travail, tout en n'oubliant pas Titouan et Inès.

Je remercie mes collègues neurochirurgiens sans qui ni l'envie ni l'aboutissement de cette recherche n'auraient été possibles.

Je remercie l'équipe de MediCis, fidèle équipe de recherche depuis mon master II: équipe sans cesse en renouvellement, faisant toute sa richesse et assurant la pérennité de sa qualité au fil du temps.

Je voudrais aussi remercier très chaleureusement l'équipe du McConnell Brain Imaging Centre admirablement dirigée par Pr Louis Collins. C'est en son sein que j'ai pu construire la première et solide pierre de cette thèse.

Je remercie Xavier Morandi et Pierre Jannin pour leurs soutiens et leurs aides en tant que directeur et co-directeur de ma thèse.

Un grand merci aux anciens de MediCIS partis au loin: Bérengère Aubert-Broche, Daniel Garcia-Lorenzo, Pierrick Coupé, Caroline Essert, Florent Lalys, Tiziano d'Albis, et à tous ceux que j'oublie.

Construction et validation d’une base de données multimodales pour la stimulation cérébrale profonde

Construction and validation of a multimodal database for deep brain stimulation

Table of contents

Abbreviations

AC, anterior commissure

ANIMAL, automatic nonlinear image matching and anatomical labelling

BET, brain extraction tool

CT, computed tomography

DBS, deep brain stimulation

Dopa, dopamine

GPm, medial globus pallidus

HAC, hierarchical ascendant classification

ICBM, international consortium brain mapping

MDRS, Mattis dementia rating scale

MINC, medical Image NetCDF format

MNI, Montreal neurological institute

MRI, magnetic resonance imaging

PC, posterior commissure

PD, Parkinson's disease

STN, subthalamic stimulation

SyN, Symmetric Image Normalization technique

T1w or T2w, weighted-T1 or T2 MRI

UPDRS III, (motor) part III of the unified Parkinson's disease rating scale

VLc, caudal part of the ventro-lateral thalamic nucleus

Abréviations

GPm, globus pallidus médial

IRM, imagerie par résonance magnétique

NST, noyau subthalamique

SCP, stimulation cérébrale profonde

VLc, partie caudale du noyau thalamique ventro-latéral

Introduction

High frequency Deep Brain Stimulation (DBS) is an effective treatment for patients with severe disabled movement disorders refractory to medical treatments. Developed since 1987 by Pr Benabid at Grenoble [8], DBS targets basal ganglia in the brain to stop the invalidating symptoms of the disease, but without stopping disease progression. In basal ganglia, three nuclei are most often targeted: the caudal part of the thalamic ventro-lateral nucleus (VLc), the medial globus pallidus (GPm), or the subthalamic nucleus (STN). VLc stimulation is effective on tremor whatever its origin [51]. The GPm stimulation is effective on dystonia, and on akineto-hypertonic and dyskinesias symptoms of Parkinson's disease (PD). STN stimulation is effective on any PD symptoms. Although DBS is effective on motor symptoms, it may induce adverse motor, neuropsychological or psychiatric adverse side-effects as has often been demonstrated in the literature [13,32,88,104].

DBS surgery consists of the accurate implantation of an electrode in the targeted nucleus. The quality of results of DBS surgery depends on various factors during the different steps of the procedure. Under local anesthesia, a stereotaxic frame is fixed to the patient's head and a stereotaxic 3D image is acquired. The neurosurgeon then targets one or two basal ganglia nucleus(ei) defined preoperatively according to strict clinical criteria. In the operative room, the patient, weaned off therapeutics since the previous day, is awakened so as to allow clinical tests of the effect of the stimulation and to optimise the location of the DBS electrode in the targeted nucleus. As demonstrated in the literature [7,8,38,112,113], the quality of the clinical improvement, as well as the existence of post operative motor, neuropsychological or psychiatric side effects strongly depends on the location of the electrode, and therefore on the quality of the surgical planning.

The quality of the surgical planning can be improved by developing a multimodal database based on anatomical, clinical and electrophysiologial data [27-29,40,41]. This thesis examines the different steps in the building and validating of our multimodal database on

DBS. The first step was to develop a specific magnetic resonance imaging (MRI) template of PD patients' anatomy, and to validate the basal ganglia segmentation made on this template. The second step was to study the outcome of patients with PD stimulated on two targets, the STN or the GPm by analysing anatomo-clinical atlases.

Presentation of the studies is preceded by a description of the current state of knowledge and followed by general conclusions including the future developments.

Current state of reflection

PD is recognized as one of the most common neurological disorders, affecting 1% of people over the age of 60 years. It is the second most prevalent neurodegenerative disorder. One of the characteristics of PD is the apoptosis of the dopamine-rich neurons of the substantia nigra. Major symptoms are indeed characterized by abnormalities of motor functions, several of which predominate, but all do not systematically occur in all individuals. These PD-related symptoms can be treated with medical therapy, but when it remains ineffective in some cases, DBS surgery [10,53] may be necessary according to strict patient inclusion criteria. This iterative procedure, initially approved by the Federal Drug Agency in U.S. in 1997 for essential tremor disorders, and in 2002 for PD, has gained much interest over the past decade and is now widely used by a large number of neurosurgical departments. The DBS anatomical target is based on the relief of symptoms and results of previous implantations only. The three major targets chosen by neurosurgeons according to the patients' symptoms are the VLc, the GPm and the STN. Among these three deep brain structures, the STN has become the most common target of high-frequency DBS in patients with severe motor disabled symptoms and no cognitive impairment [7-9,43,61,107].

Surgical procedure

During routine DBS surgery, two main stages are involved: pre-operative planning and the surgery itself. Pre-operative planning is the process of loading the pre-operative patient's medical images (Computed Tomography and/or MRI), recording them together and proposing a 2D and/or 3D visualisation interface to define the target localisation in the Anterior and Posterior Commissures (AC-PC) plan. Given contrast and spatial resolution limitations, the usual DBS targets are not easily visible on the MR images available to the surgeon, even though MRI offers better contrast than other medical imaging techniques [31]. Neurosurgeons directly localize the optimal target position on the T2 MR image and choose the trajectory of the electrode according to the patient's anatomical information. During this step, the additional help of an atlas may be necessary. In practice, experts manually localize AC-PC coordinates, midsagittal points and entry on the MR images of the patient. Finally,

coordinates are automatically put in AC-PC space, then computed in a stereotactic coordinates system.

The surgical procedure is then performed under local anaesthesia. The trajectory estimated during planning is implemented with stereotactic frame based or frameless systems and used as an initial position that has to be refined. A few causes of discrepancy between chosen target and the final implant may appear, such as brain shift [48,85], or patient's anatomical variability. An X-ray evaluation is thus performed intra-operatively to confirm the initial placement and evaluate potential biases. Electrophysiological explorations are also performed to help neurosurgeons refine the placement of active electrode contacts. Similarly, neurologists may test the clinical effects with different settings for each contact to reach optimum placement. Changing frequency, voltage, stimulated contact and electrode trajectory, they reach optimum placement. Lastly, the surgeon anchors the electrode to the skull.

Even though STN DBS has demonstrated its efficiency for motor symptoms improvement, questions remain concerning contact location providing the greatest motor improvement while producing the minimal neuropsychological and psychiatric side effects. Indeed, despite satisfactory motor improvements, several studies have reported adverse events after DBS surgery affecting cognitive functions, emotion or behaviour [13,32,45,88,104]. In particular, Brücke et al. [15], Greenhouse et al. [38], Kühn et al. [54], LHommée et al. [67] or Mallet et al. [71] elucidated the role of STN in emotional processing, showing that STN DBS leads to behavioral complications. Similarly, Burrows et al. [16] were interested in complications of STN DBS around the zona incerta, and York et al. [113] looked at neuropsychological complications according to electrode location and trajectory. All these results suggest that the STN forms part of a broadly distributed neural network encompassing the associative and limbic circuits. Lenglet et al. [66] studied the basal ganglia and thalamic connections using high-resolution MR images in 4 healthy subjects and concluded that it was possible to delineate the connections between the basal ganglia. As outlined above, one of the major challenges in DBS is the identification of the target, which requires additional information and knowledge for indirect identification of such small structures during the pre-operative stage with the support of digital atlases.

Atlases

Brain atlases and atlas-based segmentation techniques have been developed to facilitate the accurate targeting of deep brain structures in patients with movement disorders [7,20,58,97,103,112]. Some digitized atlases aim at providing information with optimum spatial and intensity resolution, to allow better identification of structures, which is impossible with usual medical imaging techniques only. Histological atlases were thus created [19,112] along with high-resolution MR based atlases [4,59]. Both types of atlas have been successfully introduced in the targeting stage of standard DBS procedures.

The concept of probabilistic functional atlases, built from a population of previous surgical cases, was initially introduced by Nowinski et al. [79-81]. After a process of normalization within a common space, effective contacts are linked to preoperative electrophysiological recordings and clinical scores acquired during the stages of the procedure. Statistical techniques are used to study anatomical or functional variability between patients. Response to stimulation, electro-physiological recordings and clinical scores related to motor or cognitive evolution are all potential data that can be integrated into such atlases. This fusion of clinical and anatomical information allows an understanding of functional organization within deep-brain structures that helps in the identification of the optimal therapy zone for future patients. Finnis et al. [34] and Guo et al. [40] proposed probabilistic functional atlases by integrating intra-operative recordings. D'Haese et al. [27,28] and Pallavaram et al. [84,85] proposed a system to automatically predict the optimum target position according to atlases built from retrospective studies. More recently, D'Haese et al. [29] proposed a fully integrated computer-assisted system called CRAnialVault. The system addresses the issue of data administration during the different stages of the therapy. It permits the centralisation of various types of data acquired during the procedure and provides data visualisation through data processing tools. A preliminary validation process in a clinical context, from planning to programming, is described and shows that the system provides genuine assistance to the surgical team. Evaluation of DBS electrode implantation involves significant motor and neuropsychological follow-up estimated by clinical tests. Resulting clinical scores allow post-operative evaluation of the decrease in motor disorders and possible clinical side effects. Quantitative analysis of these data relative to the actual anatomical area stimulated would provide a better understanding of the DBS phenomenon, optimization of targeting and consequently better patient outcome.

First study: automated segmentation of basal ganglia and deep brain structures in MRI of Parkinson's disease

Automated segmentation of basal ganglia and deep brain structures in MRI of Parkinson's disease

Claire Haegelen [1,2], M.D.
Pierrick Coupé [1,3], Ph.D.
Vladimir Fonov [1], Ph.D.
Nicolas Guizard [1], M. Sc.
Pierre Jannin [2], Ph.D.
Xavier Morandi [2], M.D.
D. Louis Collins [1], Ph.D.

[1] McConnell Brain Imaging Centre, Montreal Neurological Institute, 3801 University Street Montreal, QC, H3A 2B4, CANADA
[2] INSERM, U746, Faculty of Medicine, INRIA, VisAGeS Unit/Project, CNRS, UMR 06074, IRISA, University of Rennes1, CS 34317, 35043 Rennes cedex, FRANCE
[3] LaBRI CNRS, UMR 5800, University of Bordeaux, 351 cours de la Liberation, 33045 Talence cedex, FRANCE

Corresponding author: Dr Claire Haegelen, Service de Neurochirurgie, Hôpital Pontchaillou, rue Henri Le Guilloux, 35033 Rennes cedex 9, France, Email: Claire.HAEGELEN@chu-rennes.fr

KEY WORDS: Basal ganglia, MRI template, Patch-based method, Parkinson's disease, Segmentation

Running title: Segmentation of basal ganglia

Abstract

Purpose.

Template-based segmentation techniques have been developed to facilitate the accurate targeting of deep brain structures in patients with movement disorders. Three template-based brain MRI segmentation techniques were compared to determine the best strategy for segmenting the deep brain structures of patients with PD.

Methods.

T1-weighted and T2-weighted MR image templates were created by averaging MR images of 57 patients with Parkinson's disease. Twenty-four deep brain structures were manually segmented on the templates. To validate the template-based segmentation, 14 of the 24 deep brain structures from the templates were manually segmented on 10 MR scans of Parkinson's patients as a gold standard. We compared the manual segmentations with three methods of automated segmentation: two registration-based approaches, Automatic Nonlinear Image Matching and Anatomical Labelling - (ANIMAL) and Symmetric Image Normalization - (SyN), and one patch-label fusion technique. The automated labels were then compared with the manual labels using a Dice-kappa metric and center of gravity. A Friedman test was used to compare the Dice-kappa values and paired t-tests for the center of gravity.

Results.

The Friedman test showed a significant difference between the three methods for both thalami ($p < 0.05$) and not for the subthalamic nuclei. Registration with ANIMAL was better than with SyN for the left thalamus, and was better than the patch-based method for the right thalamus.

Conclusion.

Although template-based approaches are the most used techniques to segment basal ganglia by warping onto MR images, we found that the patch-based method provided similar results and was less-time consuming. Patch-based method may be preferable for the subthalamic nucleus segmentation in patients with Parkinson's disease.

Many movement disorders are related first to PD, with symptoms that include essential tremor, rigidity, and akinesia, and less frequently to dystonia that is a syndrome of sustained muscle contractions producing writhing movements and abnormal postures, to essential tremor or to Tourette syndrome. When pharmaceutical treatments lose effectiveness, such disorders may require functional neurosurgery. In such surgeries, deep brain electrodes are implanted to inhibit the activity of target structures such as the STN, GPm, and VLc [10,51,106]. Following surgery, motor effects and neuropsychological or psychiatric secondary side effects of the stimulation may occur depending on the location and trajectory of the electrodes [88,106,113]. The patient's surgical outcome is related to the accuracy of nucleus targeting during surgery, and the accuracy of electrode implantation depends on different steps such as image preprocessing, intraoperative clinical testing of patients, and intraoperative electrophysiological recordings.

Brain atlases and atlas-based segmentation techniques have been developed to facilitate the accurate targeting of deep brain structures in patients with movement disorders [7,19,20,58]. Recently, several authors have demonstrated improved targeting accuracy by using multimodal databases composed of anatomical and functional data [29,40,41]. In these studies, basal ganglia segmentations, the coordinates of previously implanted electrodes, and functional data (mainly intracerebral electrophysiological recordings) were aligned in a common space and overlaid on a MR image template. Although the use of multimodal images has been shown to be an effective tool in surgical planning, very few studies have correlated clinical postoperative data with anatomical data [40].

Developing a tool to improve targeting accuracy and the aggregation of anatomical and clinical data requires several steps, including the construction of a template to define a common stereotactic space, accurate and automated segmentation of target structures on the template, registration of the patient's multimodal image data, and alignment of the patient's image data into a common space for comparison with electrode placement. In this paper, we focus on the segmentation step by investigating the accuracy of three methods of segmenting the basal ganglia and deep brain structures of patients with PD. The goal of this work was to compare these methods and determine which method was enough accurate and clinically applicable to obtain segmentation of target structures in further patients with PD waiting for DBS.

First, we used two segmentation methods that are nonlinear registration-based approaches involving a population-specific, anatomically labeled template. This kind of approach is widely used and has demonstrated good performance in the segmentation of a large variety of structures [22]. In our study, we constructed a population-specific template [36], which has been shown to be one of the most effective methods of achieving accurate segmentation of subjects with pathology. To achieve automated segmentation, the basal ganglia and other deep brain structures useful in the planning of deep brain stimulation were first manually delineated on the template, which was then nonlinearly warped onto the patient's MR image. The segmentation of the target structures on the MR image could thus be obtained by mapping the template labels through the estimated transformation onto the patient's MR image. We compared two nonlinear algorithms to achieve this task: the well-known Automatic Nonlinear Image Matching and Anatomical Labelling (ANIMAL) method [22] and the more recent Symmetric Image Normalization (SyN) technique [5]. The third segmentation method evaluated here was a recently published, patch-based, label fusion technique that has demonstrated very good performance for hippocampus and ventricle segmentation [25]. We compared the results if the three segmentation methods in terms of anatomical similarity with the template segmentation and discussed interest of these methods in clinical practice for deep brain stimulation.

Materials and methods

Patients

The template was constructed using T1-weighted (T1w) and T2-weighted (T2w) MR images from 57 patients with Parkinson's disease. The patients (26 females, 31 males; mean age (± standard deviation) 58.9 ±8 years; mean disease duration 12.2 ±5 years) underwent electrode implantation in the STN, GPm, or VLc according to their disease (Table 1).

TABLE 1. Demographic and clinical data for 57 patients with Parkinson's disease.

target	side	number of patients	mean age (years)	sex	mean disease duration (years)
VLc	1 bilateral 4 left/ 2 right	7	65.1	3 F, 4M	12.4
GPm	24 bilateral	24	60.2	12 F, 12 M	12.6
STN	26 bilateral	26	56.1	11 F, 15 M	11.7
Total		57	58.9	26 F, 31 M	12.2

VLc: caudal part of the thalamic ventral lateral nucleus; GPm: medial globus pallidus; STN: subthalamic nucleus; M: male; F: female

Before imaging, a Leksell stereotactic frame (Elekta Instruments AB, Stockholm, Sweden) was rigidly fixed on the patient's head. All MR images were acquired on a Philips Achieva 3Tesla scanner (Philips Medical Systems, Best, The Netherlands) using a transmit-and-receive head coil. After intravenous injection of gadolinium (0.2 ml/kg), the T1w data were acquired with a three-dimensional (3D) axial fast field echo sequence (TR = 9.8 ms, TE = 4.6 ms, flip angle = 8°, 256 mm field of view, 219 continuous slices, 1 mm thickness, 256×256 matrix upsampled to voxel size of 0.5×0.5×1 mm). For 42 of the 57 patients, a T2w coronal turbo spin echo sequence was acquired (TR = 3,035 ms, TE = 80 ms, flip angle = 90 °, 36 continuous slices, 1 mm thickness, 256×256 matrix upsampled to voxel size of 0.5×0.5×1 mm). The T2w image volume was centered on the thalamus. The study was approved by the local research ethics committee, and informed consent was obtained from all participants.

Construction of the Parkinson's templates

We used the procedure detailed by Fonov et al. [36] to construct multispectral, multi-subject, unbiased nonlinear average Parkinson's disease templates. The 57 T1w images were used to create the T1w Parkinson's template (PD_T1_57), and the 42 T2w images from the same subjects were used to create the T2w Parkinson's template (PD_T2_42), using the steps described below. All images were converted to the Medical Image NetCDF (MINC) format [77], the format used at our institute for image processing.

The following preprocessing steps were applied to all MR scans prior to constructing the template: (1) the program N3 was used to correct for image intensity nonuniformity [99]; (2) inter-subject linear image intensity normalization was achieved using linear histogram scaling to the International Consortium Brain Mapping (ICBM152) template [36] following the technique of Nyul et al. [82]; (3) intra-subject inter-modality volume registration of T2w and T1w MR images was achieved with a rigid-body transformation (i.e., only 3 translations and 3 rotations) and a mutual-information cost function [110] implemented in the *mritoself* tool from the MINC mni_autoreg software package [21]; (4) inter-subject spatial alignment to the Talairach-like ICBM152 stereotactic space was achieved with a linear (nine parameter) transformation estimated with *mritotal*; and (5) a patient-specific brain mask was created by applying Brain Extraction Tool (BET) from the Oxford centre of Functional MRI of the brain Functional Software Library (FSL) to the T1w data [100]. Then, the T1w and T2w data for all subjects were intensity normalized and spatially aligned within the ICBM152 stereotactic space.

After preprocessing, the average high-signal-to-noise T1w and T2w templates were created using an iterative unbiased method [36] (see Figure 1). At each iteration, all T1w datasets are nonlinearly registered to an intermediate target and then averaged together on a voxel-by-voxel basis. The inverse of the average nonlinear transformation is applied to the intermediate template to remove any potential spatial bias. This procedure is repeated multiple times in a hierarchical fashion, gradually increasing the resolution of the nonlinear transformations, with number of iterations estimated empirically to achieve good results from a similar dataset. The result is an unbiased, high-contrast, highly detailed T1w average MR image template. Nonlinear registrations were obtained with the ANIMAL procedure [22], chosen because of our extensive experience with this technique. Following the unbiased non-linear registration, the transformations estimated on the T1w data were applied to the patient's corresponding T2w data to create the unbiased T2w average template. The templates (PD_T1_57 and PD_T2_42) enable visualization of deep brain structures such as amygdala or hippocampus and basal ganglia structures such as subthalamic nucleus or thalamus. These structures have either T1w contrast or T2w contrast, or are visible in both modalities, and can be manually segmented on each slice of the PD_T1_57 and/or PD_T2_42 templates.

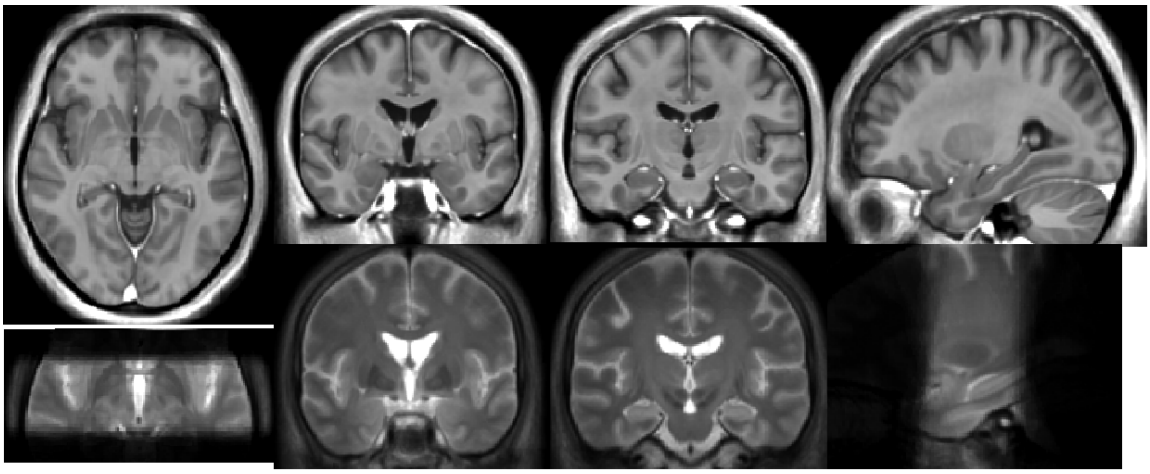

Figure 1. Parkinson's templates obtained from 57 T1w and 42 T2w average MR images of patients with Parkinson's disease. *From left to right*: Axial, coronal, coronal and sagittal slices of the T1w (*top*) and T2w (*bottom*) templates.

Manual segmentation

Manual segmentation of the template was achieved using the MNI Display software (Montreal Neurological Institute, Canada, www.bic.mni.mcgill.ca/ServicesSoftware) by the first author, Claire Haegelen. Segmentation consisted of manual delineations of 24 structures bilaterally on each slice of the PD_T1_57 and PD_T2_42 templates. The Display software allows the user to paint the structure in any chosen slice (e.g., transverse) with simultaneous update in the other two views (e.g., coronal and sagittal), enabling consistent segmentation in 3D while viewing either template. The 24 structures were identified with the help of anatomical atlases [69,97,103]. The structures were defined bilaterally and included the amygdala, hippocampus, caudate nucleus, putamen, GPm and lateral globus pallidus, thalamus, medial and lateral geniculate bodies, red nucleus, substantia nigra, and STN (see Figure 2). All the structures were visible on the PD_T2_42 template. While a rapid 36-slice T2w image, centered on the thalamus was acquired on the morning of the PD surgery, it did not permit to identify for segmentation the entire caudate nucleus, amygdala and hippocampus. For this reason, these structures were segmented on the PD_T1_57 template where they were visible. Display allows both T1w and T1w images to be visible simultaneously to ensure label consistency. It took 120 hours to manual segment the structures on the templates.

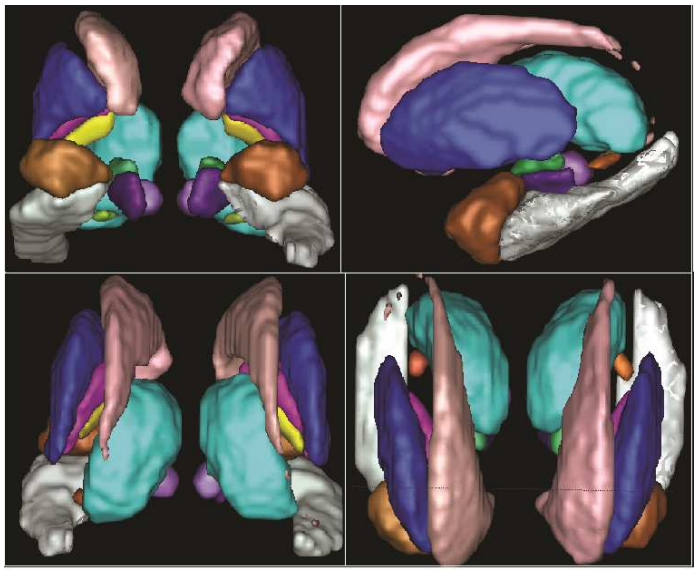

Figure 2. Anterior (*top left*), lateral left (*top right*), posterior (*bottom left*) and superior (*bottom right*) 3D views of the manual segmentation of the Parkinson's templates. The painted structures included bilateral amygdala (*brown*), hippocampus (*white*), putamen (*dark blue*), GPm (*yellow*), lateral globus pallidus (*dark pink*), caudate nucleus (*light pink*), thalami (*light blue*), substantia nigra (*dark violet*), STN (*dark green*), red nucleus (*light violet*), and medial geniculate body (*light green*).

To validate the automated template-based segmentation procedure, a gold standard labelling of patient data was required. Fourteen bilateral structures were manually painted on the T1w and T2w images of 10 patients with Parkinson's disease. The images used were a subset of those used for the Parkinson's templates after N3 nonuniformity correction [99]. Using the Display program, the structures labelled included the amygdala, hippocampus, putamen, thalamus, red nucleus, substantia nigra, and STN (see Figure 3). As for the template, the amygdala and hippocampus were segmented on the patients T1w image, and the remaining structures on the T2w image. We chose these nine structures for their different sizes: large (e.g., thalamus and hippocampus), intermediate (e.g., amygdala and putamen), and small (e.g., red nucleus, substantia nigra, and STN). The five remaining structures (caudate nucleus, GPm and lateral globus pallidus, medial and lateral geniculate bodies) were not identified on the patient scans.

To measure the quality of the manual segmentation used as a gold standard, two experts (Claire Haegelen and Louis Collins) segmented the putamen, subthalamic nucleus and

substantia nigra, on both the left and right sides, on the MRI of one patient. These segmentations were used to estimate the intra- and inter-rater variability in structure segmentation.

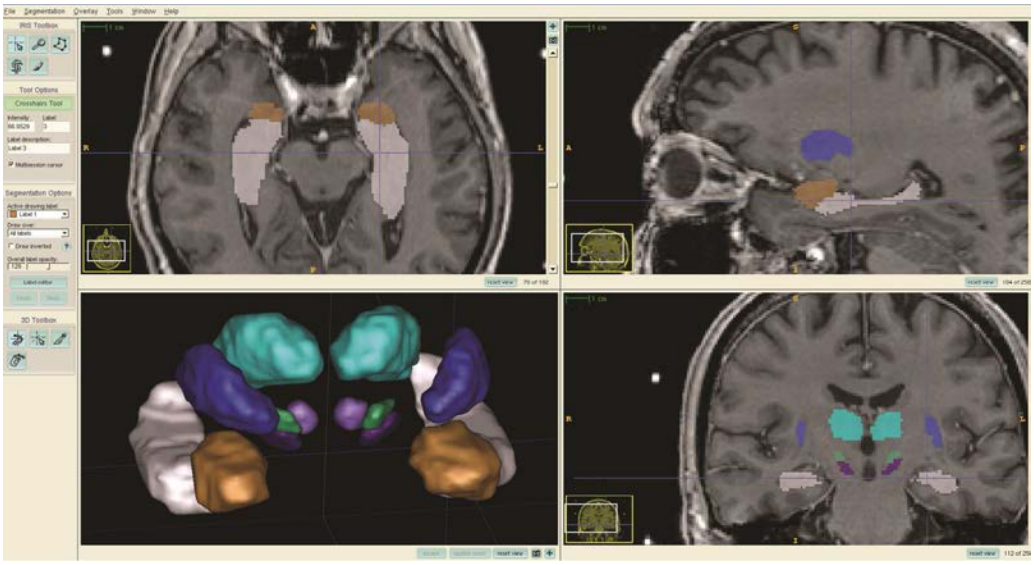

Figure 3. Screenshot of a patient's manual painting using ITKsnap. Axial (*top left*), sagittal (*top right*), and coronal (*bottom right*) slices of MR image and 3D (*bottom left*) view of the following bilateral painted structures: amygdala (*brown*), hippocampus (*white*), putamen (*dark blue*), thalami (*light blue*), substantia nigra (*dark violet*), STN (*dark green*), and red nucleus (*light violet*).

Registration with ANIMAL and SyN

As described earlier, the registration-based segmentation procedure maps the labels from the PD_T1_57 template onto the MR image using the nonlinear registration transformation that aligns the template and patient MR image data. The template's labels, customized to the anatomy of each patient, can then be compared with the gold standard labels described above. Two methods of inter-subject nonlinear registration were evaluated: ANIMAL [22] and SyN [5]. So, as not to bias the comparison between the two methods, only the T1w modality was used to drive the non-linear registration. Furthermore, the PD_T1_57 template was more appropriate for the whole-brain registration since the PD_T2_42 only covered part of the brain.

Linear and nonlinear transformations were calculated between the PD_57_T1 template and each patient's T1w image with both ANIMAL and SyN, resulting in two spatial warping transformations. Then, the template's labels were mapped through each of the two transformations onto the patient's T1w image to achieve two automatic structure segmentations: one for ANIMAL and one for SyN (see Figure 4).

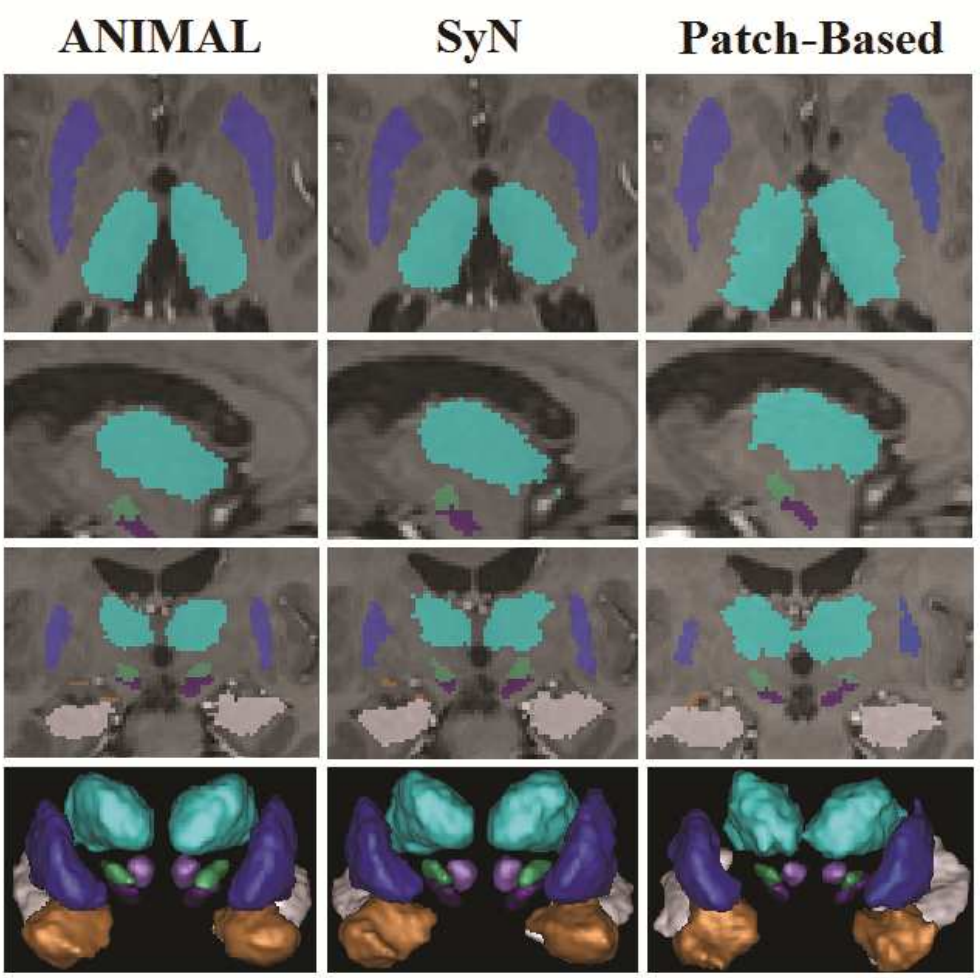

Figure 4. Generation of labels by ANIMAL registration, SyN registration and patch-based method. All labels are shown on axial (*top row*), parasagittal (*second row*), and coronal (*third row*) slices of a T1w map and on a 3D reconstruction (*bottom row*). Labelled structures: bilateral amygdala (*brown*), hippocampus (*white*), putamen (*dark blue*), thalami (*light blue*), substantia nigra (*dark violet*), STN (*dark green*), and red nuclei (*light violet*).

Patch-based segmentation method

In addition to the registration-based methods, we also evaluated a novel patch-based method using anatomical information derived from manual segmentations by experts, as described in detail in Coupe et al. [25]. This method required only linear registration into the MNI space of the involved images (i.e., subject under study and the training templates) as well as a denoising step with the 3D blockwise nonlocal means filter [114]. In brief, for each voxel in the MR image that needs to be segmented, the neighbourhood of the voxel is compared with similar neighbourhoods in previously labelled MR image datasets that serve as a library of templates. A weight, proportional to the neighbourhood similarity between the image and the templates, is computed and used as a label voting mechanism to achieve segmentation. In this manner, anatomically similar neighbourhoods from one or more templates in the library can contribute to the labelling of the patient's MR image. Here, the gold standard labels are used to define the template library, and experiments are completed in a leave-one-out fashion (i.e., the patient being tested is removed from the template library, and the remaining patients form the library).

For each patient, the patch-based method was used to obtain the same labels as those identified manually for the gold standard. We first processed the method on the T1w images of the 10 patients, but the substantia nigra, red nuclei, and STN were only visualized on the T2w sequences. For these six labels, the patch-based method was applied to the T2w images using the T2w data from the gold standard template library. Finally, the eight labels obtained from the T1w patch-based procedure and those obtained from the T2w patch-based procedure were combined to complete the patch-based segmentation for each patient. Figure 4 presents a view of the different labels obtained with the patch-based method.

Quality of fit metrics

Finally, the automatic labels obtained with either ANIMAL, SyN, or the patch-based method were compared with the manual labels of the gold standard using two metrics: the Dice's kappa similarity coefficient (kappa) [30] because this metric is well established in the literature for comparison between two segmentations and a center of gravity metric because this will yield a more intuitive estimate of the potential targeting error. We did not estimate a Hausdorf distance or edge-based/border-based distances because these can be too variable, as they are driven by extreme outlier values. The kappa was measured as follows:

$$K=2* (V(M \cap A))/(V(M)+V(A))$$

where M is the set of manually labeled voxels, A is the set of automatically labeled voxels, ∩ is the set intersection operator, and V(•) is the volume operator. K takes on a value between 0 and 1.0, with 1.0 indicating perfect agreement. Before the kappa metric is used to evaluate the automated methods, it was first used to estimate intra- and inter-rater variability of manual structure segmentation to establish a baseline for comparison.

The center of gravity was estimated for each segmented structure obtained with the 3 methods, the ANIMAL and SyN registrations and the patch-based method. The Euclidean co-ordinates of the center of gravity were used to estimate a distance between the automatic segmentations and their respective gold standard. A paired-t test was used to compare the distances obtained with ANIMAL and SyN and with the patch-based method. A *p*-value of less than 0.05 was deemed significant. We also computed the center-of-gravity values between the repeated manual segmentations of the two experts, to estimate inter-rater variability.

Data analysis

The resulting kappa values were not Gaussian distributed; therefore, a nonparametric Friedman test for paired data was used to compare the kappa values obtained with ANIMAL and SyN and with the patch-based method. A *p*-value of less than 0.05 was deemed significant. When a significant difference was detected by the Friedman test, a nonparametric post-hoc multicomparison test was used to determine which pair of methods was significantly different.

Results

The results of intra- and inter-rater variability of manual segmentation are presented in Table 2. The results of the center-of-gravity values between the deep brain structures obtained with 2 registration methods and the patch-based method are presented in Table 3.

TABLE 2. Mean kappa values for comparison of segmentation of three cerebral structures by two experts, each segmentation made three times on the same patient with Parkinson's disease.

	Inter-rater		Expert 1		Expert 2	
	Mean	**SD**	**Mean**	**SD**	**Mean**	**SD**
Putamen	0,77	0,04	0,83	0,03	0,84	0,02
SN	0,68	0,02	0,80	0,03	0,79	0,02
STN	0,55	0,08	0,71	0,07	0,74	0,02

SN, substantia nigra; STN, subthalamic nucleus; SD, standard deviation.

TABLE 3. Mean distances and standard deviation (in mm) between the center of gravity positions between manually segmented deep brain structures, and the automatically segmented labels from the 3 different methods: ANIMAL, SyN and the patch-based method.

	Distance	
	Mean	**SD**
ANIMAL	1.51	0.88
SyN	1.48	0.92
Patch-Based Method	1.29	0.76

SD, standard deviation.

The paired-t test showed a significant difference between the SyN registration and patch-based method ($p = 0.01$) and the ANIMAL registration and patch-based method ($p = 0.002$). There was no difference between ANIMAL and SyN registration methods in terms of distances ($p = 0.13$). The mean distances measured between the repeated segmentations of the two experts were 0.82 (standard deviation (SD) 0.49) and 0.96 (SD 0.36) for respectively Claire Haegelen and Louis Collins. These mean distances were not significantly different ($p = 0.15$).

The kappa index values obtained with the three methods are presented in Table 4 and Figure 5.

ANIMAL and SyN-based method: The median kappa values computed between the labels obtained with ANIMAL and the manual labels were greater than 0.73 for the bilateral thalami, putamen, amygdala, hippocampus and red nuclei, and between 0.62 and 0.67 for the bilateral substantia nigra and subthalamic nuclei (Fig. 5).

Patch-based method: The median kappa values computed between the labels obtained with the patch-based method and the manual labels were greater than 0.76 for the bilateral thalami, putamen, amygdala, hippocampus, and red nuclei, and between 0.62 and 0.70 for the bilateral substantia nigra and subthalamic nuclei (Fig. 5).

The Friedman test showed a significant difference between the three methods for the left amygdala ($p = 0.014$), left red nucleus ($p = 0.045$), and left ($p = 0.045$) and right thalamus ($p = 0.001$) (Fig. 6). For the left amygdala, the patch-based segmentation method was better than with ANIMAL. For the left red nucleus and left thalamus, registration with ANIMAL was better than with SyN. For the right thalamus, registration with ANIMAL was better than the patch-based method.

TABLE 4. Dice-kappa values for three methods of segmentation of 14 cerebral structures in 10 patients with Parkinson's disease.

	l_AG	r_AG	l_HC	r_HC	l_put	r_put	l_thal	r_thal	l_RN	r_RN	l_SN	r_SN	l_STN	r_STN
ANIMAL														
Mean	0.760	0.759	0.763	0.743	0.815	0.809	0.864	0.868	0.796	0.793	0.689	0.657	0.641	0.640
Median	0.773	0.738	0.792	0.760	0.814	0.809	0.854	0.858	0.781	0.774	0.671	0.640	0.624	0.638
Variance	0.0016	0.0007	0.002	0.0012	0.0012	0.0014	0.0008	0.0007	0.0027	0.002	0.0015	0.0033	0.004	0.006
SyN														
Mean	0.776	0.760	0.774	0.760	0.816	0.809	0.854	0.858	0.781	0.782	0.671	0.640	0.626	0.64
Median	0.776	0.759	0.792	0.771	0.814	0.809	0.854	0.867	0.792	0.782	0.671	0.640	0.624	0.65
Variance	0.0013	0.0005	0.003	0.0013	0.0009	0.0013	0.0008	0.0008	0.0030	0.0029	0.0009	0.002	0.003	0.006
Patch-based														
Mean	0.780	0.739	0.764	0.767	0.825	0.795	0.850	0.828	0.790	0.783	0.696	0.653	0.631	0.575
Median	0.810	0.761	0.780	0.766	0.822	0.790	0.851	0.819	0.785	0.784	0.704	0.675	0.621	0.626
Variance	0.008	0.005	0.0002	0.0001	0.005	0.0006	0.0006	0.0008	0.002 [a]	0.003 [a]	0.003 [a]	0.009 [a]	0.005 [a]	0.022 [a]

[a] Values according to the automatic method only on the T2w analysis; l, left; r, right; AG, amygdala; HC, hippocampus; put, putamen; thal, thalamus; RN, red nucleus; SN, substantia nigra; STN, subthalamic nucleus

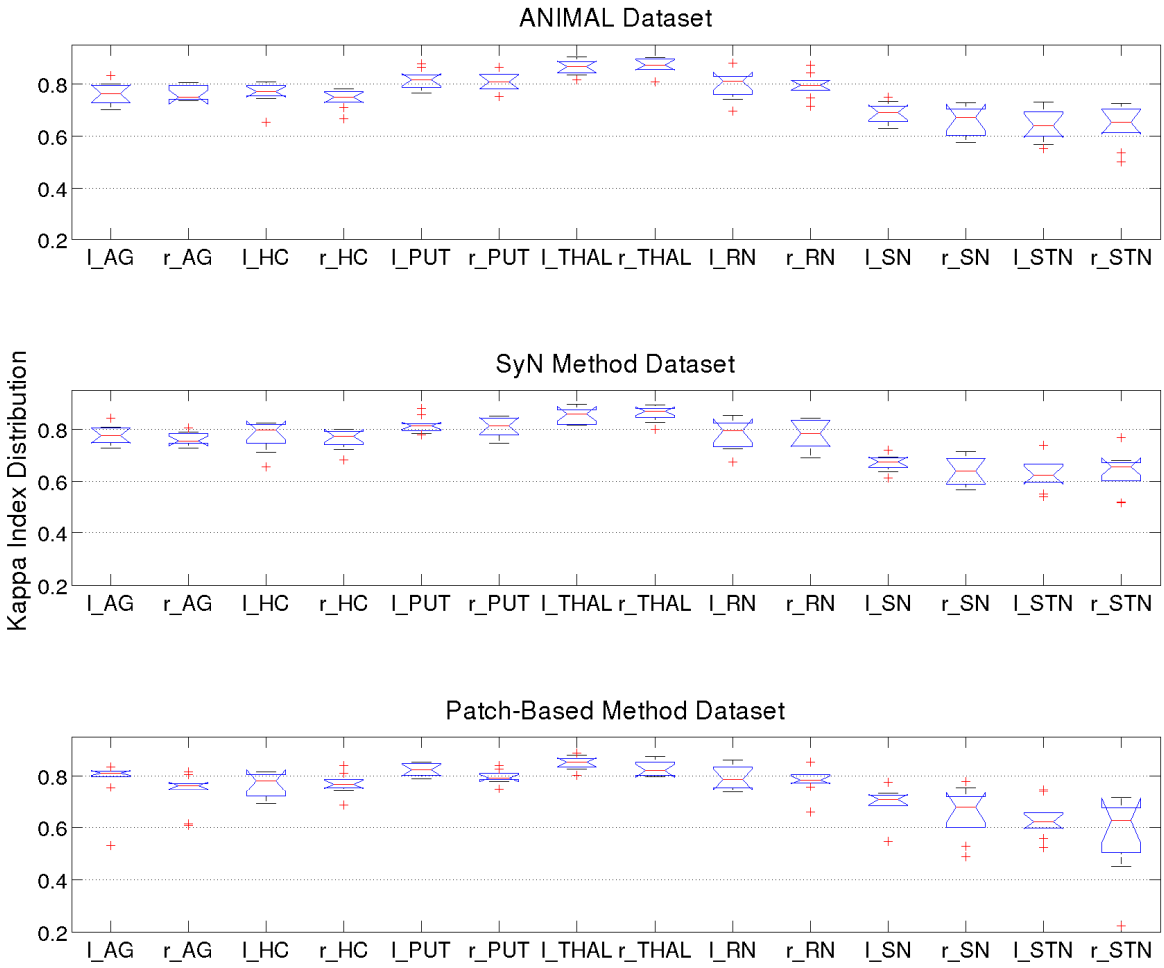

Figure 5. Box plots of the kappa index distribution for ANIMAL registration (*top row*), SyN registration (*second row*), and patch-based method of segmentation (*bottom row*). Boxes represent the lower quartile, median (*red line*), and upper quartile of the kappa index distribution. Whiskers show the most extreme values within 1.5 times the interquartile range. Outliers (*red* +) are data with values beyond the ends of the whiskers.

l_AG: left amygdala; r_AG: right amygdala; l_HC: left hippocampus; r_HC: right hippocampus; l_PUT: left putamen; r_PUT: right putamen; l_THAL: left thalamus; r_THAL: right thalamus; l_RN: left red nucleus; r_RN: right red nucleus; l_SN: left substantia nigra; r_SN: right substantia nigra; l_STN: left subthalamic nucleus; r_STN: right subthalamic nucleus.

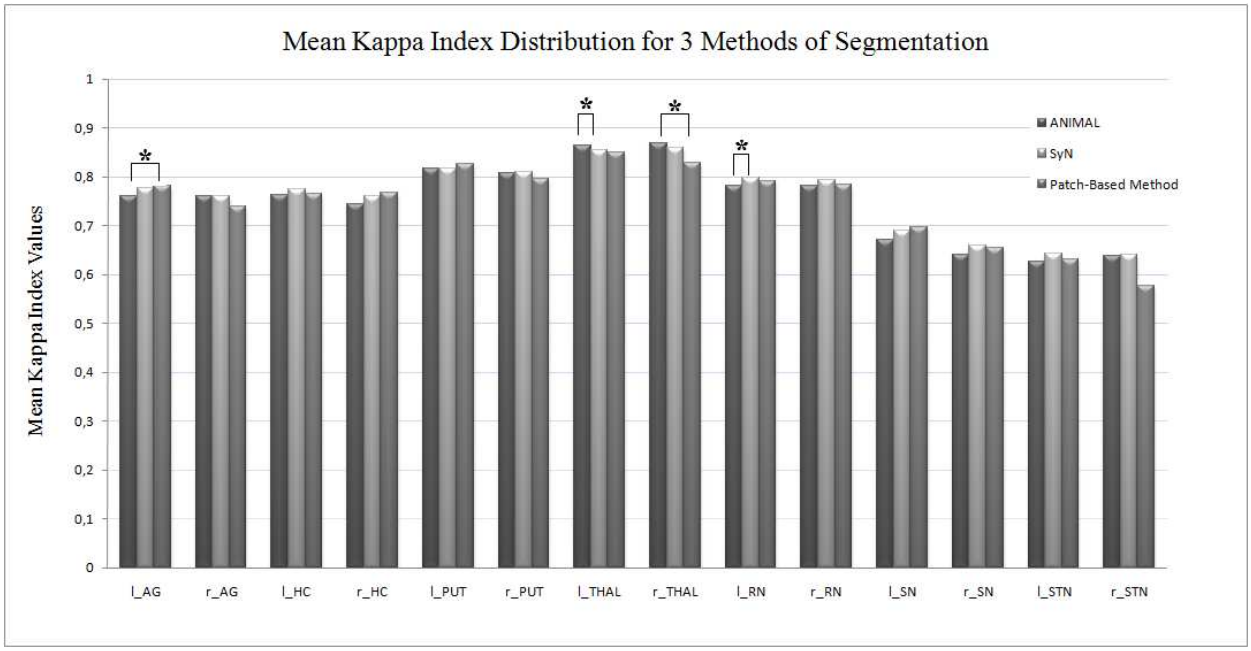

Figure 6. Mean kappa index distribution for segmentation of cerebral structures in 10 patients with Parkinson's disease using ANIMAL registration, SyN registration, and patch-based method. ***** represents a significant difference between two methods according to Friedman and post hoc multi-comparison test (see the text in RESULTS for details).

Discussion

The template-based segmentation approach is one method that has been developed to assist neurosurgeons in the target planning step of deep brain stimulation procedures. For example, Bardinet et al. [7] and Chakravarty et al. [19] developed different 3D histological atlases that were aligned to a MR image of the same brain obtained after autopsy, and to an average MR image, respectively. The template can then be registered to the patient's MR image to delineate deep brain structures like the STN or GPm that will be targeted during surgery. We built a high-resolution/high-signal-to-noise ratio template by averaging the nonlinearly aligned MR images of many patients with Parkinson's disease. This process allowed us to obtain T1w and T2w templates with a high degree of anatomical detail for deep brain structures and the cerebral cortex. In contrast to the atlases of Bardinet et al. [7] and Chakravarty et al. [19], we have a direct high-quality visualization of the basal ganglia on the PD_T1_57 template and even more so on the PD_T2_42 template for those nuclei that are only visible on the T2w images, such as the red nucleus, substantia nigra, and subthalamic nucleus (see Figure 1). The segmentation of the basal ganglia and deep brain structures is an important step in obtaining their 3D representation and importing them onto the patient's MR image. The manual segmentation of deep brain structures by the first author, Claire Haegelen, was found to be easier on the PD_T1_57 and PD_T2_42 templates than on a 3T digitized mono-subject template [58] obtained from a normal subject, but this fact was difficult to quantify and demonstrate, and beyond the scope of this paper where the goal was to compare three segmentation procedures. One of the limits of our study was that the segmentation used during methods comparison was performed by only one expert. However, the segmentation quality was verified by a second expert, Xavier Morandi and two experts (Claire Heagelen and D. Louis Collins) repeatedly segmented three cerebral structures of a patient with Parkinson's disease to estimate intra- and inter-rater reliability (see Table 2). The intra-rater segmentation reliability was quite high with values above 0.83 for putamen, around 0.80 for substantia nigra, and between 0.71 and 0.74 for the STN. The inter-rater segmentation variability was slighty higher than the intra-rater for putamen and SN while significantly higher for STN. This suggests that the manual delineation of STN from T1w MR scan is a very challenging task due to low contrast and small structure size that limits the possible consensus between expert's segmentations. Moreover, the manual segmentation of putamen, SN and STN in patients with Parkinson's disease is difficult because these patients have a

specific pathological loss of neurons of these three structures affecting their MRI visualization. In the literature, very few studies have done manual segmentation of basal ganglia from MRI or on histological slides [7,19] because of the great anatomical variability and the lack of very specific MRI sequences to identify accurately the STN, SN and putamen in patients with basal ganglia pathologocial changes like those seen in Parkinson's disease. In the literature, many segmentation methods [23,25,46,89] are first tested on lateral ventricles, hippocampus or amygdala, structures for which the boundaries and limits are better defined. In our opinion, these facts explain why in our study the STN had higher inter-rater variability compare to other reports of automatic segmentation techniques. Considering these manual segmentation difficulties, our results should be taken with the caveat that the inter-rater variability is relatively high. Nevertheless, the mean distances between centers of gravity were not different in the two sets of manual segmentations, and these distances were lower in labels obtained with the patch-based method than with the two registration methods. Furthermore, the mean Dice Kappa values for inter-rater segmentation are at approximately the same level as the mean Dice Kappa values comparing the manual labels and those generated by the three automatic techniques. In the future, we will investigate the effect of consensus segmentations from multiple experts.

To our knowledge, this is the first study to compare different registration approaches and the patch-based method to identify deep brain structures in the context of Parkinson's disease. We applied two nonlinear registration-based segmentation tools to MR images, as nonlinear registration has been shown to perform better than linear registration for the automated identification of subcortical targets [6,12,19]. The accuracy of the automated segmentation depends on the accuracy of registration. In Klein et al. [50], the two nonlinear tools, ANIMAL and SyN, were assessed based on overlap measures of manually labelled anatomical regions, as was done in our study. SyN was one of the methods that reached top rank for all label sets [50]. In our case, the two nonlinear registrations were quite similar for all the structures, even for the smallest ones, except for the left thalamus and red nucleus, for which ANIMAL performed better than SyN. The advantage of this type of segmentation approach is that the manual segmentation is performed on a high-contrast image (i.e., the template), which facilitates the delineation procedure. However, the difficulty is then in registering the template with an individual MR image because of inter-subject variability. A linear (or affine) transformation consists in transforming a template into the image space of

the patient's MR data. Although it can account for variations in size, orientation, and position, a linear transformation cannot radically alter the shape of the template as is needed to account for anatomical differences between the patient's image and the template. Instead, nonlinear transformations are needed to address this issue. By using nonlinear transformations, we obtained a more accurate segmentation result; however, the nonlinear registration of the template to the patient MR image is time consuming, taking in our case from thirty minutes to one hour per patient for ANIMAL and from one to three hours per patient for SyN.

Another way to obtain better segmentation accuracy than by registering images to a single labelled template is to fuse several labelled images [23]. Fusing the labelled images in the training library can be done by nonlinear registration [2,23] or patch comparison [25]. The advantage of label fusion approaches is that they can handle inter-subject variability correctly by aggregating labels from several images. In this manner, different anatomical patterns can be optimally fused to fit the patient's anatomy. The patch-based label fusion approach evaluated here is also less time consuming than nonlinear registration, since it required only one minute of processing.

The difficulty with the patch-based label fusion approach is that it requires manual segmentation of structures on the MR images of several subjects to form the library. Not only is this task time consuming, but it is also difficult due to low image contrast, especially in the context of Parkinson's disease where motion artefacts greatly impact the image quality. While the overall segmentation quality was similar for the patch-based and registration-based methods, there was more variability in the segmentation quality of the patch-based approach (see Figure 5 and Table 4). As shown in Coupe et al. [25], the quality of the segmentation of patch-based label fusion depends on the number of training templates in the library. During our leave-one-out experiment, only nine templates were used to segment the subject under study. This number of training templates is small compared with what is suggested in Coupe et al. [25] (between 20 and 30). By increasing the number of training templates, the segmentation quality is expected to increase and the robustness of the segmentation to improve.

The kappa metric is often used to compare the agreement between structures in the literature [2,19,23,25,89]. The kappa metric depends on the surface-to-volume ratio of the structure, with decreasing kappa values in small structures for which the ratio increases. We found lower kappa values for the hippocampus than what is reported in Coupe et al. [25] ($\kappa = 0.884$) and Collins et al. [23] ($\kappa = 0.887$), and also for the amygdala, for which Collins et al. [23] found ($\kappa = 0.826$). As mentioned, this lower segmentation quality may be due to the smaller number of training subjects used in our segmentation procedure. It might also be due to the low-contrast images of patients with Parkinson's disease or to the use of a different database [23,25]. Patenaude et al. [89] used a Bayesian appearance model approach to provide accurate segmentation of 15 subcortical structures on 336 manually labelled T1w MR images. They found that the best structures in terms of kappa values were the thalamus and putamen with a median kappa as high as 0.85, and the hippocampus with a median kappa between 0.80 and 0.85, as in our study, though we found lowest kappa values for the same structures. Patenaude et al. [89] found that the worst structures in terms of kappa values were the amygdala and the nucleus accumbens because, in those cases, the kappa penalized small structures or structures with a higher surface-to-volume ratio. We also found lower median kappa values for the smallest structures, the STN and substantia nigra, but not for the red nucleus. One hypothesis may be that, in patients with Parkinson's disease, compared with the red nucleus, the STN and substantia nigra are more affected by the loss of dopaminergic neurons and therefore more difficult to identify with automated segmentation tools.

The three methods were relatively equivalent in terms of mean and median kappa values, suggesting they perform similarly in producing the automated segmentation of deep brain structures. Differences between the three methods were observed only for some of the structures, which mean there was, in fact, very little dissimilarity. However, when applied to a new patient, the patch-based method is notably more efficient than the other two methods, as it avoids the lengthy time-consuming non-linear registration step to achieve segmentation. Moreover, considering the resulting high inter-rater variability in our study, the automatic segmentation was as variable as another expert rater but was not subject to intra-rater variability. The patch-based method probably underestimates the size of the labels because of the mean center-of-gravity values between the labels lower than with the two other registration methods. The STN deep brain stimulation proved a great efficacy in reducing symptoms of Parkinson's disease [3,76]. The patch-based segmentation method may improve

the surgical workflow by quickly and automatically identifying the STN on the preoperative MRI data of new patients, thus reducing part of the preoperative planning time in STN targeting. In clinical practice, the patch-based method is not yet applicable because it requires an engineer. From a point of view of a neurosurgeon, the three methods of segmentation were accurate enough to visualize the STN or the thalamus and to be applicable to new patients. The limits were the long time consuming step of the ANIMAL and SyN registrations method in clinical practice. More work is needed to have a software solution that is usable by the clinicians without supervision of the engineers.

Conclusions

We have developed the first step toward a multimodal database on deep brain stimulation, specifically, the construction of an MR image template specific to Parkinson's disease, and also evaluated a method of achieving the accurate segmentation of the basal ganglia and deep brain structures on patient data.

We compared three methods to determine the best strategy for segmenting the basal ganglia and deep brain structures on patients' MR images. We assessed that the intra-rater variability between the manual segmentations was lower than the inter-rater variability. Although template-based approaches are the most frequently used techniques to warp basal ganglia segmentation onto MR images, we found that the patch-based method provides similar results and is much less time consuming.

Second study: Anatomo-clinical atlases in subthalamic stimulation

Anatomo-clinical atlases using clinical data and electrode contact coordinates: application to subthalamic deep brain stimulation

Florent Lalys [1,2] Ph.D

Claire Haegelen [1,2,3] M.D

Maroua Mehri [1,2] M.Sc

Sophie Drapier [4] M.D

Marc Vérin [4] Ph.D

Pierre Jannin [1,2] Ph.D

[1] INSERM, LTSI U1099, Faculté de Médecine CS 34317, F-35043 Rennes Cedex, France

[2] University of Rennes I, F-35042 Rennes, France

[3] Department of Neurosurgery, Pontchaillou University Hospital, F-35043 Rennes, France

[4] Department of Neurology, Pontchaillou University Hospital, F-35043 Rennes, France

KEY WORDS: Deep brain stimulation, Parkinson disease, anatomo-clinical atlas, medical imaging

Running title: Anatomo-clinical atlases in subthalamic stimulation

Abstract

Purpose.

For patients suffering from PD with severe movement disorders, functional surgery may be required when medical therapy isn't effective. In DBS, electrodes are implanted within the brain to stimulate deep structures such as STN. The quality of patient surgical outcome is generally related to the accuracy of nucleus targeting during surgery.

Methods.

In this paper, we focused on identifying optimum sites for STN DBS by studying symptomatic motor improvement along with neuropsychological side effects. We described successive steps for constructing digital atlases gathering patient's location of electrode contacts automatically segmented from postoperative images, and clinical scores. Three motor and five neuropsychological scores were included in the study. Correlations with active contact locations were carried out using an adapted hierarchical ascendant classification. Such analysis enabled the extraction of representative clusters to determine the optimum site for therapeutic STN DBS. For each clinical score, we built an anatomo-clinical atlas representing its improvement or deterioration in relation with the anatomical location of electrodes and from a population of implanted patients.

Results.

To our knowledge, we reported for the first time a discrepancy between a very good motor improvement by targeting the postero-superior region of the STN and an inevitable deterioration of the categorical and phonemic fluency in the same region.

Conclusion.

Such atlases and associated analysis may help better understanding of functional mapping in deep structures and may help pre-operative decision-making process and especially targeting.

As far as we know, no atlases have yet been proposed for representing the relationships between the STN anatomy and a broad panel of pre- and post-operative clinical scores. While most of these atlases use a single motor score for modelling the global outcome of the patient, e.g. Guo et al. in 2006 [40], we proposed in this paper to extend this research by adding pre- and post-operative motor, cognitive and neuropsychological scores of patients with Parkinson's disease and inclusion criteria for subthalamic stimulation. We thus introduce the concept of anatomo-clinical atlases and describe the methods for their computation. A high-resolution mono-subject template, already validated in the context of DBS [58], and a multi-subject template [42] were tested as common spaces. Three motor and five neuro-psychological scores were then used to create anatomo-clinical atlases. The correlation was carried out using a dedicated non-supervised classification system and enabled the extraction of representative clusters to determine the optimum site for therapeutic STN DBS.

Materials and Methods

The purpose of this study was to correlate and represent the anatomical position of electrode contacts with clinical outcomes in STN DBS. Firstly, a method for automatic extraction of electrode contacts for each patient was developed. Secondly, an accurate patient images-to-template registration step was studied. Thirdly, the integration of clinical scores from a clinical database was used to extract representative anatomo-clinical clusters, through non-supervised classification.

Data

The study population consisted of 30 patients (14 women and 16 men, mean age: 60 +/- 5 years) with idiopathic PD who had bilateral STN DBS according to selected inclusion [52,61,62]. In particular, one of the inclusion criteria is the improvement of 50% in UPDRS III score during the pre-operative levodopa challenge test. All patients had one pre-operative 3-T T1-weighted MR (Size: 256 x 256 x 182, resolution: 1 mm x 1 mm x 1 mm, Philips Medical Systems) and two CT scans (Size: 203 x 203 x 155, resolution: 0.44 mm x 0.44 mm x 0.6 mm, in post-operative acquisition and 0.5 mm x 0.5 mm x 0.6 mm in pre-operative acquisition, GE Healthcare VCT 64). Pre-operative scans were acquired after attachment to the patient's head of a stereotactic Leksell frame, under local anaesthesia. All images were de-

noised using the Non-local means algorithm [24] and a bias correction algorithm based on intensity values [72] was also applied to MR images. This study was part of a larger clinical study approved by the local ethical review board.

To assess the global patient outcome, we first chose three motor scores: the UPDRS III (Unified Parkinson's Disease Rating Scale, part III) score [33], the Schwab & England [98] scale, and the Hoehn & Yahr [44] scale. For each score, patients were tested without medication (Dopa Off) immediately prior to surgery (DBS Off) and three months after it under stimulation (DBS On), also without medication. We then selected five neuropsychological scores:

- The categorical and the phonemic verbal fluency tests [18] that determine the ease with which patients can produce words.
- The Stroop test [102] that computes the mental vitality and flexibility
- The Trail Making Test [92] that determines visual attention and task switching.
- The Wisconsin Card Sorting Test [78] that estimates the ability to display flexibility in the face of changing schedules of reinforcement.
- The Mattis Dementia Rating Scale (MDRS) [73] that tests global cognitive efficiency.

Contact localization

For each electrode, the spatial coordinates of the contacts were automatically computed from post-operative CT images by modelling the electrode's axis. We developed a new segmentation technique based on the hypo-signal artefacts (white artefacts) created on CT scans and corresponding to the electrodes. Every CT scan was first simply linearly registered to a reference patient CT. On this reference image, a mask was defined including the two electrodes and entirely excluding the skull. An intensity threshold was applied in order to extract every hypo-signal voxel of both electrodes per patient. Along with a connected component approach for retrieving noise, for each slice, the barycentre of extracted voxels was computed to model the electrodes' axis. By keeping 10 mm from the tip of the electrode, we then performed regression in order to model the area where contacts can finally be obtained by applying geometry constraints of electrode 3389 from Medtronic NeuroModulation, USA (Figure 1). This automatic procedure was performed for post-operative CT of each patient and gave us all contact locations. It was validated in Mehri et al. [75] and gave us an error of 0.96 ± 0.33mm using a linear regression for the modelling of the electrode's axis.

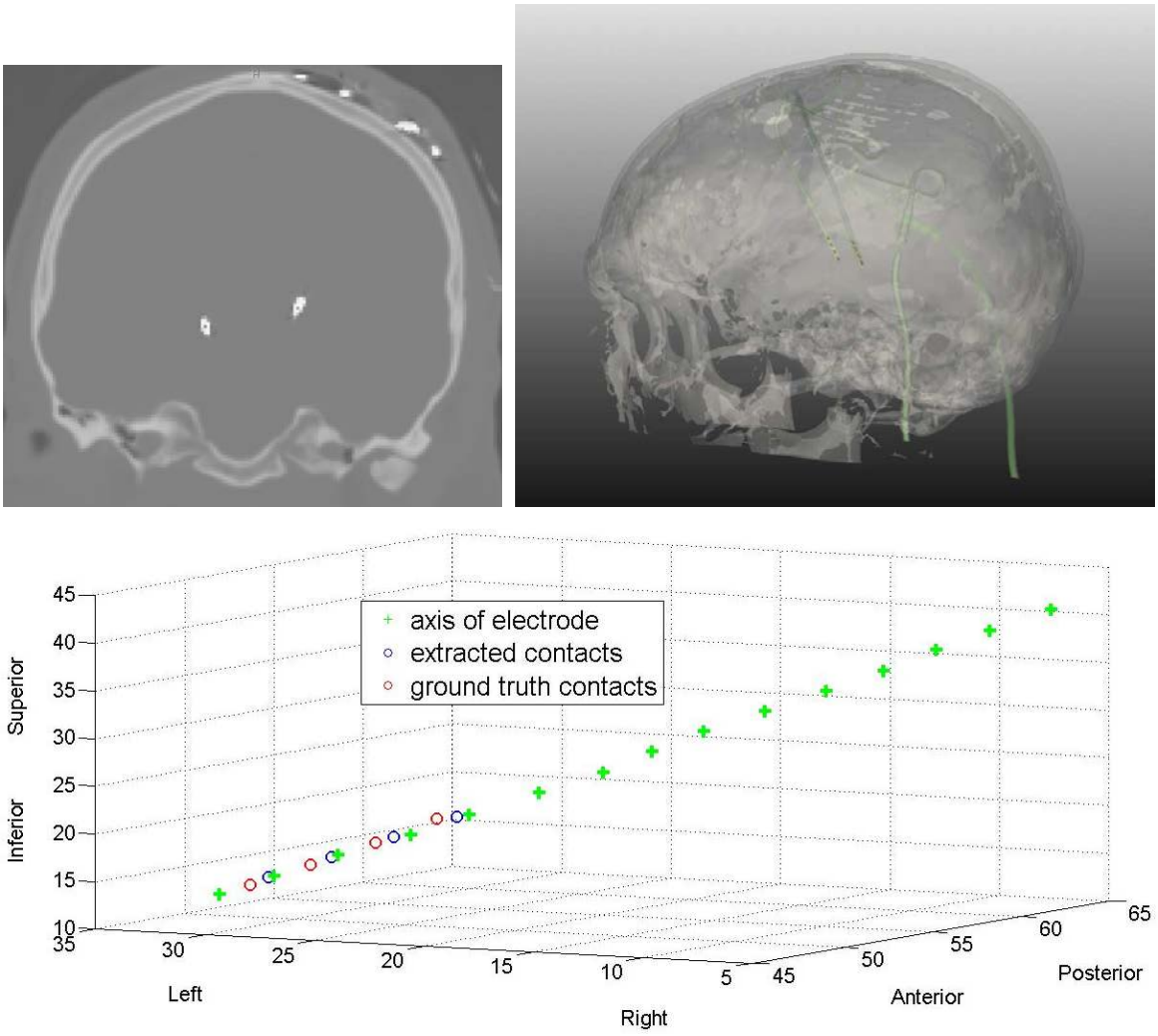

Figure 1. *Upper left*: Post-operative CT scan of one patient with PD and bilateral STN-DBS. *Upper right*: Segmentation of the patient's skull, the 2 electrodes and the 8 electrode contacts. *Below*: Electrode's axis, the 4 extracted contacts and the 4 ground truth contacts for the left side.

Patient to template registration workflow

Patient contacts were warped into a MR template as a common anatomical space for allowing retrospective population statistical analysis. We compared the impact of mono-subject vs. multi-subject MR high-resolution templates on the patient/template non-linear

registration accuracy. In opposition to pure histological templates, MR templates are correctly representing the *in vivo* anatomy of the brain. We also compared two non-linear registration methods.

The mono-subject template was created from 15 3T MR acquisitions of a healthy 45 year-old male, which were processed and averaged. This high-resolution 3T MRI template (namely the Jannin15), was constructed and assessed by Lalys et al. [58]. The multi-spectral multi-subject, unbiased non-linear average, PD template was made from 57 T1w images of patients with PD (namely the PD_T1_57), thus providing a high-resolution / high signal-to-noise ratio template [42]. This template allows the specific developmentally important age-ranges and atrophy of PD patients to be taken into account.

The registration workflow was composed of a linear CT to MR patient images registration, a global affine MR-to-template registration, a local affine MR-to-template registration with a mask on deep structures, and a final non-linear registration. Using this procedure the contact positions could be precisely warped into a reference space. We compared the accuracy of two non-linear registration algorithms: the demons approach (*www.itk.org*) that was used in our previous studies, and the Advanced Normalization ToolS non-linear deformation algorithm used in Symmetric Normalization (SyN) mode that has been shown to be highly effective in the context of MR brain imaging registration [50].

For both validation studies, we followed a landmark-based validation approach. Ten anatomical structures were identified within deep-brain structures (Figure 2) and manually identified in the images by an expert. Placement of these landmarks on the one hand on the template, and on the other hand on 15 wrapped MR images, allowed us to compute a global registration error. Considering that the intra-subject registration between the CT scan and the MR image was accurate, we only validated the MR-to-template registration. We first compared both templates by keeping the classical linear registration process along with the non-linear Demons algorithm. We then compared, using the best template found, both non-linear registrations (i.e. Demons vs SyN) using a Student t-test.

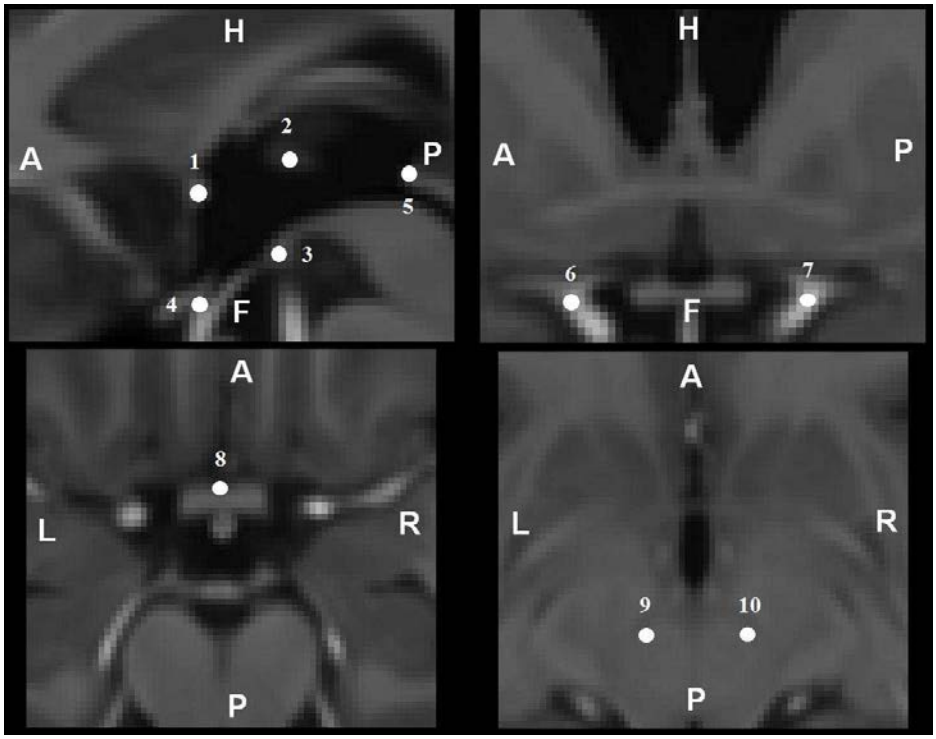

Figure 2. Anatomical landmarks used for the validation study showed on a median sagittal (*top left*), coronal *(top right*), and two axial slices (*bottom*) of the PD_T1_57 template.

1 - Anterior Commissure

2 - Interthalamic adhesion on the middle of the axial slice

3 - Posterior Commissure

4 - Infundibular recesse

5 - Middle of the mamillar bodies

6,7 - Left and right internal carotid division into anterior and middle cerebral arteries

8 - Center of the anterior portion of the optic chiasma

9,10 - Centers of the left and right red nuclei

A, anterior; P, posterior; L, left; R, right

Anatomo-clinical atlases

For all scores and for representing the degree of improvement or worsening of the patient, the difference between DBS ON and DBS OFF values was computed. In order to represent all improvement or worsening of patients on a similar scale, all clinical scores were statistically normalized. On each score, we subtracted the mean and divided by the variance of the dedicated score. After normalization, the data closely followed a normal distribution (with

mean=0 and standard deviation=1) and were more easily usable for data variation comparisons.

For each score, an atlas was computed as the list of active contact coordinates from all patients associated with the corresponding difference value. The active contacts were those at three months post-surgery. 3D visualization consisted in displaying the list of points represented with a colour code related to the patient clinical scores. Each clinical score can therefore create one anatomo-clinical atlas. Due to random errors or missing values in reporting scores, the initial clinical score dataset of 30 patients dropped to 23 for the motor analysis, but remained at 30 for the neuropsychological analysis.

Non-supervised classification

After atlas construction, we performed a segmentation step using non-supervised techniques. Hierarchical Ascendant Classification (HAC) was used on clinical scores merged with coordinates to search homogeneous groups of patients and extract general clinical trends. Feature vectors were composed of four features: the value of the x-axis, y-axis, z-axis and the score difference value. HAC operates by successively merging pairs of existing clusters, where the next pair of clusters to be merged is chosen as the pair with the smallest distance. This linkage between clusters *a* and *b* was performed using the Ward criterion along with the weighted Euclidean distance:

$$d^2(a,b) = n_a n_b \frac{\sum_{k=1}^{M} w_k \left| \overline{x_{ak}} - \overline{x_{bk}} \right|}{n_a + n_b}$$

where $\overline{x_a} = \frac{1}{n_a} \sum_{i=1}^{n_a} x_{ai}$ is the centroid of cluster a (resp. b), n_a (resp. n_b) is the number of objects in cluster a (resp. b), and w_k are the weights, specified by $w_1 = w_2 = w_3 = \frac{1}{12}$ and $w_4 = \frac{3}{4}$. The dendrogram was cut in order to obtain two or three clusters for each clinical score. Validation of the non-supervised classification was performed with an ANOVA test.

Results

The registration error was computed for the different combinations of non-linear registrations and templates. First, results of Table 1 showed that the new multi-subject template was significantly better than the mono-subject one ($p = 0.025$). The Table 2 showed that the new non-linear registration method (SyN) gave best results compared to the Demons algorithm ($p = 0.05$). For the rest of the study, the two new parameters were then conserved, providing a global registration error of 0.98 ±0.17 mm.

TABLE 1. Landmark-based validation for the comparison of the Jannin15 vs. PD_T1_57 templates on patient to atlas non-linear registration using Demon's method.

	Mean registration error (mm)	SD (mm)	Student's test
Jannin15 template + Demons non-linear registration	1.23	0.12	$p = 0.025$
PD_T1_57 template + Demons non-linear registration	1.15	0.09	

mm, millimeter; SD, standard deviation

TABLE 2. Landmark-based validation for the comparison of the Demons vs. ANTS-SyN non-linear registration methods.

	Mean registration error (mm)	SD (mm)	Student's test
PD_T1_57 template + Demons non-linear registration	1.15	0.09	$p = 0.05$
PD_T1_57 template + SyN non-linear registration	0.98	0.17	

mm, millimeter; SD, standard deviation

Patient's contacts were also warped in the Talairach space for clinical verification. The origin of the electrode contact coordinates was the midpoint between the AC and the PC points. Three months after surgery, the mean position of the active electrode's contacts was:

- on the left: 14.33 mm for the lateral direction, 1.79 mm posterior to the midpoint for the antero-posterior direction, and 1 mm under the AC-PC line for the dorso-caudal direction;
- on the right: 14.65 mm for the lateral direction, 1.88 mm posterior to the midpoint for the antero-posterior direction, 0.77 mm under the AC-PC line for the dorso-caudal direction.

The mean stimulation parameters used were frequency at 130 Hz, pulse duration for 60 microseconds for all the patients and a mean voltage of 2.14 ± 0.34 V.

For all following figures, we represent the results in the Talairach space as well as in PD_T1_57 template to improve clinical representation and interpretation. For each clinical score, clustering was performed for both hemispheres independently. For each clinical score, we noticed that the group of patients (clusters) that were extracted for both hemispheres were identical. The x-axis represents the left-right direction, the y-axis represents the antero-posterior direction, and the z-axis represents the caudo-cranial direction. The scale of figures is shown in mm. Figure 3 shows a greater improvement of UPDRS III for cluster Blue compared to clusters Red and Green ($p = 10^{-6}$). Majority of the contacts of the cluster Blue were in the postero-superior region of the STN. Hoehn & Yahr and Schwab & England scores showed similar results, but with a fuzzy definition of clusters ($p = 5.10^{-2}$).

Figure 4 shows a deterioration of the categorical fluency in the posterior region (cluster Red), and an improvement in the anterior region (cluster Blue) ($p = 10^{-4}$). For the phonemic fluency we found a general deterioration for all patients, without apparent separation of clusters. STROOP score analysis (Figure 5) indicated score improvement in the postero-superior region (cluster Red), and deterioration in the antero-inferior region ($p = 10^{-5}$) (cluster Blue). For the three other neuropsychological scores (Trail Making Test, Wisconsin Card Sorting Test, MDRS score), no significant clusters were found ($p > 5.10^{-2}$). Table 3 summarizes results of the analysis using the different clinical scores.

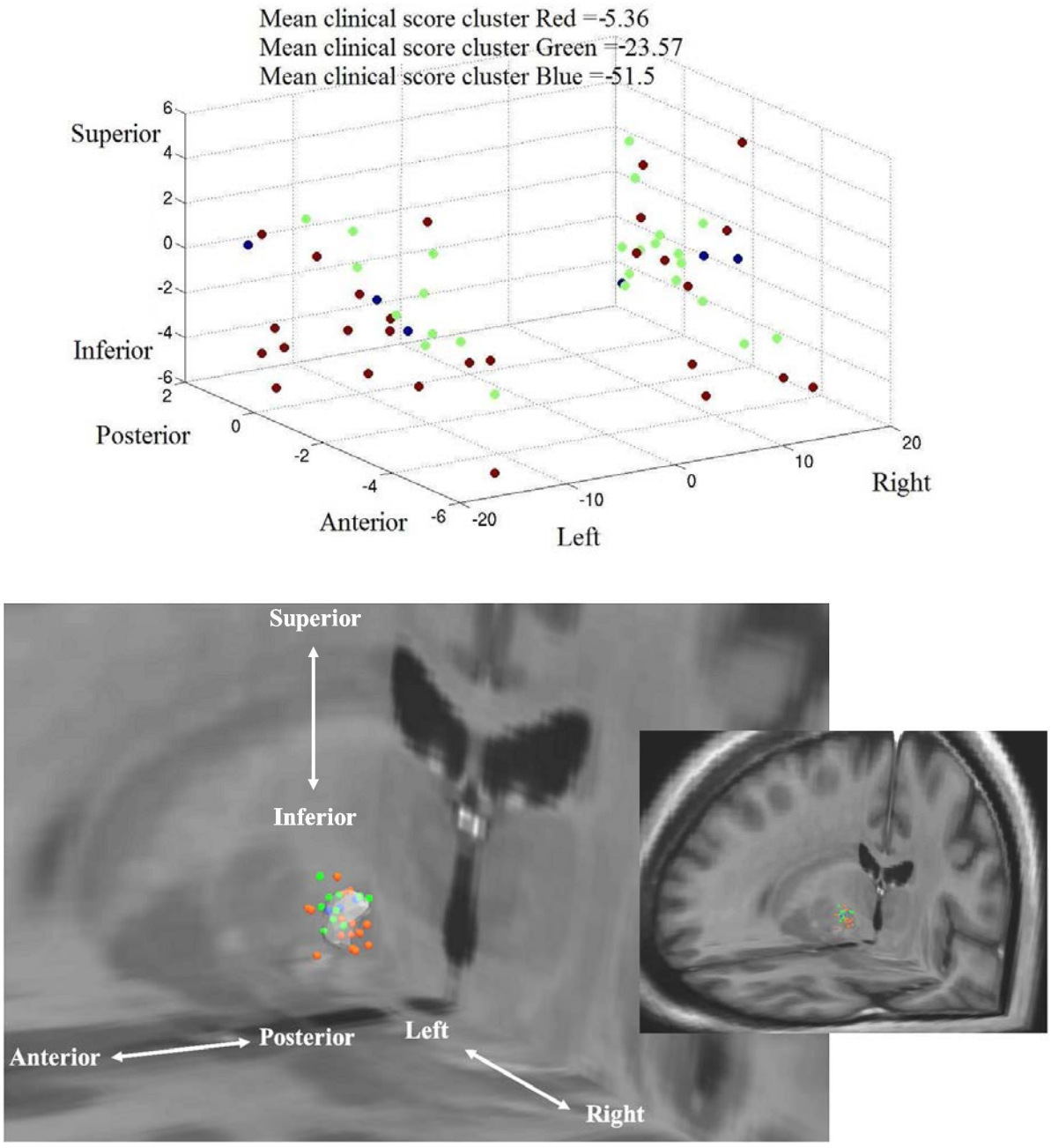

Figure 3. UPDRS III analysis, with the cluster display in Talairach coordinates (*above*), and the cluster display in the template space for the left hemisphere with the STN (*below*).

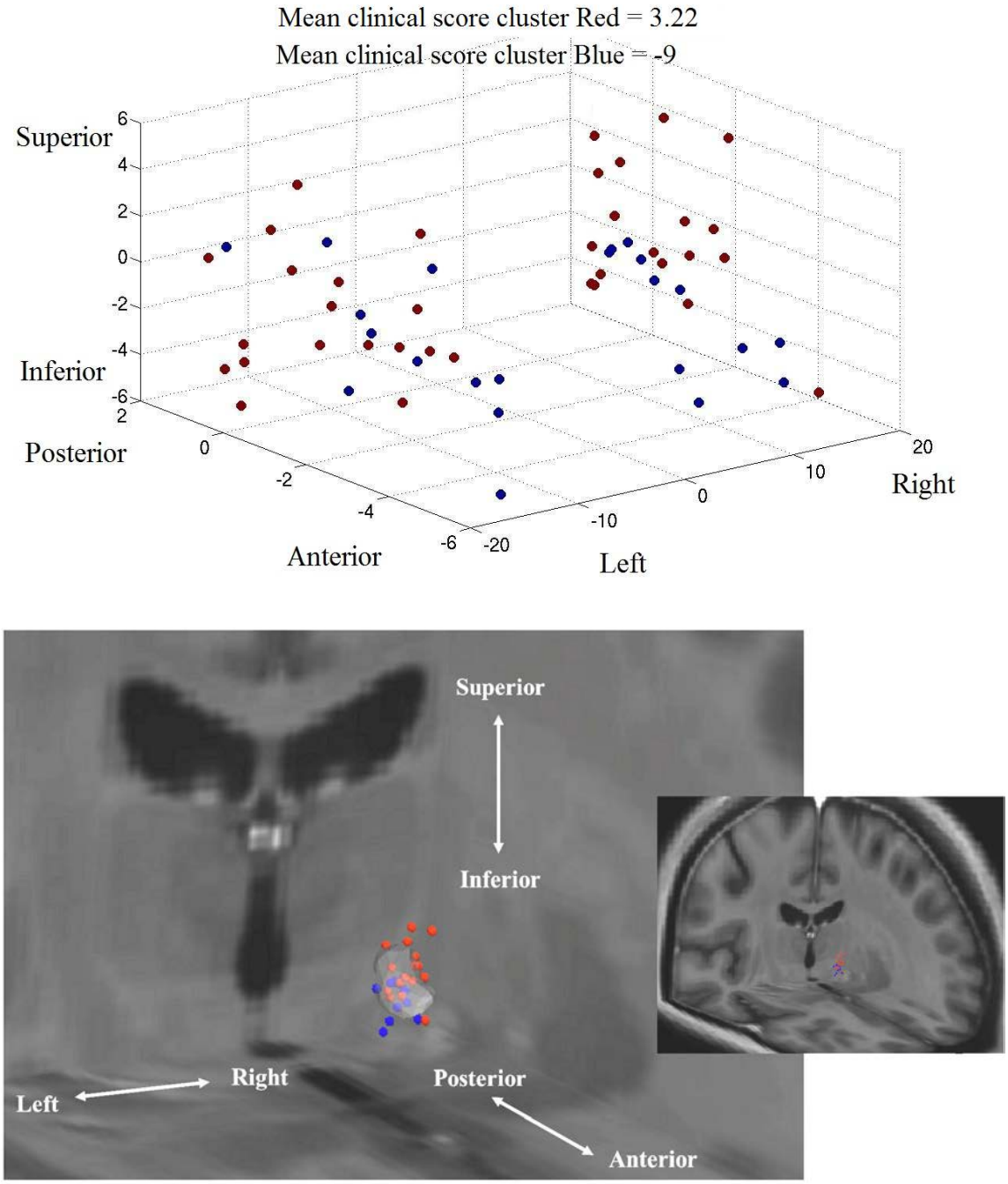

Figure 4. Categorical fluency analysis, with the cluster display in Talairach coordinates (*above*), and the cluster display in the template space for the right hemisphere with the STN (*below*).

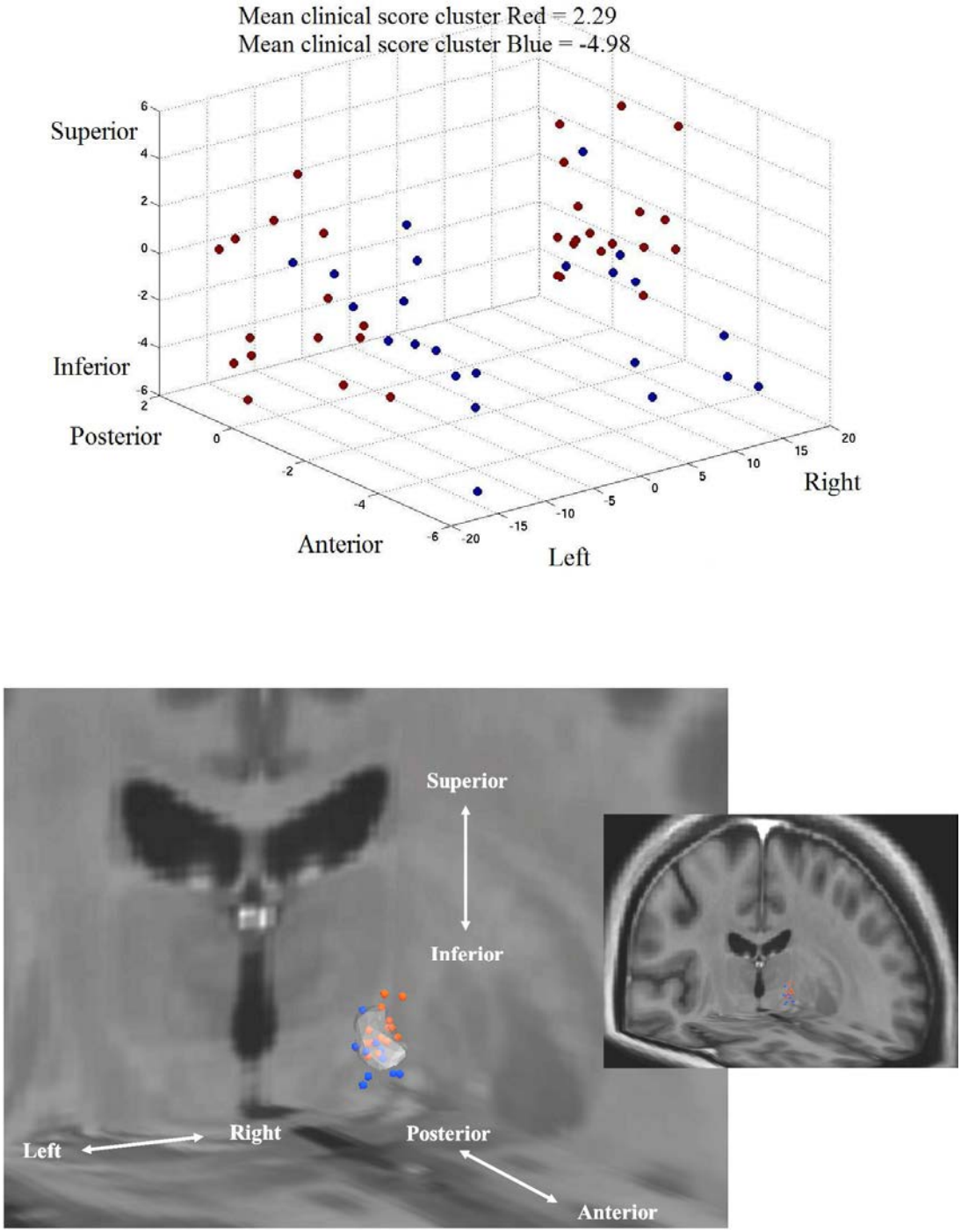

Figure 5. STROOP analysis, with the cluster display in Talairach coordinates (*above*), and the cluster display in the template space for the right hemisphere with the STN (*below*).

TABLE 3. Summarization of clusters found for each clinical score, i.e. the number of patients per cluster, the dedicated mean clinical score, the clinical signification of the mean clinical score and the major STN zone of stimulation of the patients belonging to this cluster.

Clinical scores	Cluster	Number of patients	Mean clinical score (Post-pre-op)	Clinical signification	Major STN zone of stimulation
UPDRS III	*Blue*	3	-51.5	Very good improvement	Postero-superior region
	Green	11	-23.6	Good improvement	Superior and Posterior regions
	Red	15	-5.4	Stabilisation	Anterior and inferior regions
Categorical fluency	*Blue*	11	-9	Improvement	Anterior region
	Red	18	3.2	Deterioration	Posterior region
Stroop test	*Blue*	13	-5	Deterioration	Antero-inferior region
	Red	15	2.6	Improvement	Postero-superior region
Others	No significant cluster found				

Discussion

This article reports about the construction of anatomo-clinical atlases in patients with STN stimulation and severe disabled PD. To our knowledge, we reported for the first time a discrepancy between a very good motor improvement by targeting the postero-superior region of the STN and an inevitable deterioration of the categorical and phonemic fluency in the same region. These results were provided by the use of tools already validated but never used together to provide the association of clinical scores with electrode contacts within a normalized space in the context of STN DBS.

Contact localization and representation

Many publications advocate the use of post-operative MRI to determine the electrode's contact coordinates [90,96] despite the possible adverse effects related to MRI acquisition with implanted DBS electrodes [74]. The use of MRI has recently been validated by Lee et al. [64] with a study showing that there were no significant discrepancies between the centres of electrodes estimated by CT and MRI. In this project, the spatial coordinates of the 4 contacts per electrode were automatically computed from post-operative CT images. The automatic contact localization algorithm gave us satisfactory results with an average error of 0.96 ±0.33 mm [75]. This error, even quite low, has to be taken into account in the final cluster analysis. Considering the relative small size of the STN and its sub-regions, this bias will still have to be minimized using more robust automatic segmentation algorithms. Comparison of electrode positions of STN DBS estimated in the immediate post-operative CT with those estimated 6 months after surgery showed that they may contain some discrepancies [49]. Results also indicated that it is often due to the extensive pneumocephalus. Ideally, this bias could be reduced by comparing clinical scores evaluated 6 months after the surgery with a post-operative CT acquired within the same period.

We modelled the signal by a point corresponding to the centre of the artefact. For further developments, it will be crucial to integrate the influence of stimulation on the surrounding biological tissues. Some studies on the modelling of tissues and electrical influence of electrodes in the context of DBS have recently been published [17]. Complete DBS modelling

would integrate all of these data to provide the highest possible precision.

Template and registration workflow

We compared the impact of mono-subject vs. multi-subject MR high-resolution templates on the patient/atlas non-linear registration accuracy. Both templates allowed the production of reference images with a high degree of anatomical detail, both for deep-brain structures and for the cerebral cortex. The accuracy of the patient images-to-template registration is an important step, which may considerably impact the quality of the findings. In DBS, major sources of errors are due to the identification of basal ganglia from patient-specific images. Therefore, during the procedure, we added a local registration involving targeted structure (STN), intended to improve basal ganglia registration. Results of the template-to-patient registration comparison have shown that the new multi-subject template increases the accuracy of a patient-to-template basal ganglia registration. This is explained by the fact that the single subject template did not take into account brain atrophy of the patient population. The impact of this new template was significant and it has improved not only registration quality (0.98 mm) but also retrospective visualization. During the registration workflow, intra-subject rigid registration appears to be very effective, especially when native acquisitions are subject to a step of reliable pre-processing as we performed in our registration procedure. On the contrary, the patient-to-template registration procedure, including linear and non-linear registrations steps, was subject to small errors that can explained this registration error of 0.98 mm. Similarly to the localization of the electrode contacts, this bias has to be taken into account when analysing the final cluster results.

Many active contacts are located outside the STN within atlases. This can be partially explained by the error induced during the warping step, though other explanations could be put forward. First, the electrical stimulation zone is in fact larger than the simple contact position, recovering a region wide enough to accept a targeting uncertainty. It is known, in any case, that the field of stimulation can have a spread of up to 2 mm within the brain [17]. Secondly, deep-brain tissues and nerves are deeply interconnected and nerves at the periphery of structures have an influence on the structure itself.

The coordinates of the stimulated contacts were more lateral than those previously reported [32,45,53]. One explanation could be that the targeting in our study was based on 3T MRI and not on ventriculography as in other centres. The visualisation of the STN on T2 pre-operative MRI allowed direct targeting instead of probabilistic targeting based on the Talairach atlas. The neurosurgeons attempted to place the electrode in the postero-superior part of the STN as they knew that it is involved in motor component of the STN [91,105].

Clinical scores

Each clinical score was used to extract representative clusters. Compared to clustering on clinical scores only, adding coordinates allows a better definition of clusters and a better understanding of DBS efficiency according to contact locations. Motor and neuropsychological scores were analysed to assess the patient outcome [8,9,14]. Other teams have also focused on the analysis of clinical scores in the context of STN DBS [39,63].

In our procedure, the main issue was the inability to separate the response to DBS stimulation of the right and left contacts. Each test was performed with both activated contacts. Separate evaluations would involve many hours without medication and stimulation in order to lose previous therapeutic and stimulation effects. In the pre-operative targeting procedure, surgeons first localized the optimum target position of one side, and the target position of the other side was automatically computed from the definition of the mid-sagittal line. These targets were used as an initial position that had to be refined per-operatively.

Other variables that could have been taken into account are the different contact parameters, i.e. the frequency, pulse duration and voltage. From the 30 patients in our study, these parameters did not differ among patients, so we did not include the stimulation parameters in the study. Moreover, the standard deviation of the stimulation voltage was low and not sufficiently discriminant to be included.

Because of their low granularity, values of the Schwab & England and Hoehn & Yahr scales turned out to be less representative than UPDRS III. Moreover, our method was more

useful for quantitative continuous data than for quantitative discontinuous data. For this reason, even though the results of motor scores studies were almost identical, the visualization of the atlas containing the UPDRS III provides more information. Using these clinical data, the postero-superior region has been found to be the most effective region for motor improvement. This follows conclusions of previously published work on the topic [39,63], and can be explained by the fact that this part of the STN (usually named the dorso-lateral part) is involved in sensory and motor functions [70]. Indeed, a subdivision of the STN into a ventromedial associative and a medial limbic (psychology, mood) territories is described in the literature. Recent studies [47,60] stated that the motor region was situated in the posterior portion of the nucleus. Our results related to motor improvements therefore support this hypothesis. Moreover, this subdivision can explain that the antero-inferior (corresponding to the limbic territory) region has shown significant neuropsychological side effects such as the deterioration of the Stroop score. In Lambert et al., [60], the limbic zone was found to be in the anterior portion of the STN. Results on the Stroop score are also quite satisfactory as it can be explained by recent discoveries on STN territories. Lastly, our study highlighted at our knowledge for the first time, that the categorical fluency was improved in the anterior region of the STN, whereas the categorical fluency was worse in its postero-superior region. Moreover, the phonemic fluency was worse after STN stimulation whatever the region of the STN stimulated. This last result was not surprising as the deterioration of phonemic verbal fluency is one of the most observed side effects in STN DBS, though the phenomenon is not really understood [95,104]. The deterioration of the phonemic fluency seems to be impossible to avoid after STN stimulation and the categorical fluency only improved in the anterior region that is not the best region in terms of motor improvement. We can imagine multiple sub-regions within the STN where the stimulation may involve these side effects, but the extraction of finer spatial clusters would require a larger study population. Our results could also demonstrate that the STN is not so well subdivided into three different functional territories but the motor, associative and limbic territories are more probably mixed due to diffused interneuron’s connection.

Lastly, concerning all other neuropsychological scores (Trail Making Test, Wisconsin Card Sorting Test, MDRS score), no clusters were clearly defined, resulting in small statistical differences. With our current data, no statistical clusters could be extracted from these scores yet, either because of the number of patients associated with the different bias of

the analysis, or because no significant effects were observed amongst patients for these specific clinical scores.

Conclusions

In this paper, we focused on identifying optimum sites for STN DBS by studying symptomatic motor improvement along with neuropsychological side effects. The concept of anatomo-clinical atlases, introduced in this paper, allows the integration, within a single coordinate system, of a digitized brain MRI template, previous target coordinates of implantations, and various clinical scores. Each clinical score produced one anatomo-clinical atlas, associating the degree of improvement or worsening of the patient with its active contacts. Additionally, non-supervised classification was performed on scores and coordinates to extract clusters for determining optimum electrode contact coordinates. We showed how to extract knowledge gained from population data based on the correlation between anatomical location of contacts and clinical data.

To our knowledge, we reported for the first time a discrepancy between a very good motor improvement by targeting the postero-superior region of the STN and an inevitable deterioration of the categorical and phonemic fluency in the same region. The proposed anatomo-clinical atlases were created to provide the surgeons with additional assistance for better understanding of DBS-related phenomena. It could find its application in pre-operative planning [26,101] as well as for post-operative assessment [57]. As targeting is mainly based on the surgeon's knowledge and experience, it could serve as an additional source of information obtained from retrospective studies for reducing time and predicting motor outcome and possible post-operative adverse-effects.

The underlying challenge would be to reduce the intra-operative time required for electrode contact adjustment by microelectrode recordings. The actual local anaesthesia would be replaced by a general anaesthesia, which would completely alter the surgical routine by reducing surgical staff workload, improving patient care and increasing medical safety. Alternatively, such atlases also provide an understanding of previous interventions that didn’t give satisfactory results. In such cases, active contacts of a new patient can be warped into the common space, displayed for post-operative assessment, and inserted into a new analysis for updating the atlases. This work yields many flourishing studies in the field, including further clinical data such as quality of life or cognitive criteria.

Third study: Anatomo-clinical atlases in medial pallidal stimulation

Construction of statistical anatomo-clinical maps on medial pallidal stimulation in Parkinson's disease

Claire Haegelen, M.D. [1,3,4]
Florent Lalys, Ph.D. [3,4]
Tiziano D'Albis M.D. [3,4]
Verin Marc, M.D, Ph.D. [2,5]
Drapier Sophie, M.D. [2,5]
Pierre Jannin, Ph.D.[3,4]
Xavier Morandi, M.D. [1,3,4]

Departments of Neurosurgery [1] and Neurology [2], CHU Pontchaillou, Rennes, France
[3] INSERM, LTSI U1099, Faculté de Médecine CS 34317, F-35043 Rennes Cedex, France
[4] University of Rennes I, F-35042 Rennes, France
[5] Behavior and Basal Ganglia host team 4712, University of Rennes 1, F-35042 Rennes, France

Corresponding author: Dr Claire Haegelen, Service de Neurochirurgie, CHU Pontchaillou, rue Henri Le Guilloux, 35033 Rennes cedex, Phone: +(33)2 99 28 42 77, Fax: +(33) 2 99 28 41 80, Email: Claire.HAEGELEN@chu-rennes.fr

KEY WORDS: Anatomo-clinical atlas, Deep brain stimulation, Imaging database, Parkinson disease

Running title: Anatomo-clinical maps in medial pallidal stimulation

Abstract

Purpose.

The choice between GPm and STN stimulation for PD is still controversial in the literature. The goal of this study was to analyse the clinical results and the neuropsychological impacts after pallidal medial stimulation by a new method using statistical anatomo-clinical maps.

Methods.

We studied 20 patients with PD operated on to implant GPm stimulation, 3 months before and 6 months after surgery. We developed a new analysis method based on statistical maps to correlate motor and neuropsychological scores with a 3mm zone of stimulation around the active electrode contact. All analysis was carried out on a spatially normalized reference image, i.e. a specific Parkinson template. We obtained two maps per score, one representing the number of patients per voxel, and the second one representing the change in the score with a color scale from blue to red.

Results.

We obtained five statistical maps representing the UPDRS part III, Mattis Dementia Rating Scale (MDRS), phonemic and categorical fluency and Stroop test. Overall, most of the patients were stimulated in the postero-ventral part of the GPm. The map concerning the UPDRS part III showed most of the patients improved. The MDRS map showed stability in the patients. The map concerning phonemic fluency showed a deterioration of the patients whatever the zone stimulated. The map on categorical fluency showed either deterioration or a slight improvement after GPm stimulation. The Stroop test map showed stability or an improvement after GPm stimulation.

Conclusion.

GPm stimulation is effective on motor symptoms of PD without inducing new motor and neuropsychological side effects. The best region to stimulate was the postero-ventral part of the GPm bilaterally, as demonstrated by our statistical maps. We consider it more effective to use a more lateral site than previously described in the literature.

High frequency DBS is an effective treatment for patients with severe disabled movement disorders refractory to medical treatment. For 25 years, STN stimulation has proved its efficacy on the triad of Parkinson's symptoms [8,9] notwithstanding its potential neuropsychological and psychiatric secondary effects [13,32,38,88,104]. Thus, strict inclusion criteriae have been defined for STN DBS, excluding patients with cognitive impairment and/or axial symptoms. In our center, we operated on GPm DBS patients with severe disabled PD where STN DBS was contraindicated. Rouaud et al [94] proved that GPm DBS was a cognitively safe and effective treatment for motor fluctuations and dyskinesias refractory to medical treatment, by analyzing clinical results with standard statistical tests. GPm stimulation has also proved its efficiency in treatment for severe primary dystonia [106], especially when the postero-ventral part of the GPm was stimulated. In electrophysiological and animal studies, the postero-ventral part of the GPm is known as its motor part whereas the more antero-ventral and mid sections of the GPm had respectively limbic and associative functions [86]. The GPm is larger than the STN and a controversy exists in the literature over which target in the GPm is effective in treating patients with PD without inducing other motor side effects.

Functional atlases introduced by Nowinski et al [79-81] integrate information such as position of electrode contacts, stimulation or electrophysiological recordings to determine the efficacy zones of DBS. Functional atlases have been developed in a majority of cases for STN DBS because of the small size of this nucleus and the difficulty of its direct targeting based on MRI contrast, and for better understanding of the secondary neuropsychological side effects of the stimulation. We previously described a methodology for the creation of novel functional atlases in STN DBS that correlate clinical scores with active electrode contacts in order to better understand clinical effects of stimulations according to their specific locations. In particular, we showed that targeting the postero-superior region of the STN induced discrepancy between a very good motor improvement and a deterioration of the categorical and phonemic fluency in the same region [59]. This new analysis method took into account only the representation of the stimulated contact but did not model the entire stimulation zone of each contact. In this paper we applied functional atlas to GPm DBS improving it by our new analysis method so as to better locate the effective stimulation zone in a nucleus bigger than the STN. Even if many authors [94,108,109] reported no neuropsychological deterioration after GPm DBS, we would like to analyze more accurately the effect of stimulation on neuropsychological aspects in different GPm areas.

The goal of this study was to create new statistical anatomo-clinical maps, 1) to prove the safety and efficacy of the GPm DBS in patients with severe disabled PD and contraindicated for STN DBS, and 2) to determine the best target for GPm DBS in Parkinson's disease according to the construction of motor and neuropsychological maps.

Materials and Methods

Patients and surgery

Twenty advanced PD patients, who underwent GPm DBS at our Hospital between 2006 and 2012, were enrolled in the study. All met the criteria of the United Kingdom Parkinson's Disease Society brain bank for idiopathic PD [37]. The female-to-male ratio was 12-8 with a mean age of 62.2 ±7 years and mean disease duration of 12.9 ±5.3 years. STN DBS was contraindicated for all patients, due to cognitive impairment (MDRS ≤ 130 or impaired executive functions) and/or dopa-resistant axial motor symptoms (dysarthria, freezing, falls) at baseline. After a complete description of the study, written informed consent was obtained from each participant and the study was conducted in accordance with the Declaration of Helsinki. Clinical assessment was performed before (mean 5 ±4.7 months) and after surgery (mean 6 ±2 months) and was conducted in accordance with the Core Assessment Program for Intracerebral Transplantation (CAPIT) [62] and included the UPDRS III [33], the Hoehn and Yahr (H&Y) scale [44] and the Schwab and England (S&E) scale [98]. Neuropsychological tests included the MDRS [73] for global cognitive assessment and a battery of tests assessing executive functions, including Nelson's simplified version of the Wisconsin Card Sorting Test [78], the Trail Making Test [92], the Stroop test [102], and categorical and literal fluencies [18].

For the UPDRS III score, patients were tested by a neurologist before surgery without medication (Dopa Off) and at 6 months after surgery with stimulation (DBS On) and without medication. For each neuropsychological score, patients were tested with medication (Dopa On) immediately prior to surgery and six months after it under stimulation (DBS On), also with medication.

A relative score of improvement or deterioration $S\%$ can be defined for each score S. Given that the patients were not all responding the same way to medication, an average of both scores was necessary as follow:

- for the UPDRS III:

$$S\% = \frac{S^{post}_{dopa-off-DBS-on} - S^{pre}_{dopa-off}}{S_{\max} - S_{\min}}$$

- for the other scores:

$$S\% = \frac{S^{post}_{score} - S^{pre}_{score}}{S_{\max} - S_{\min}}$$

where $S^{post}_{dopa-off-DBS-on}$ and $S^{pre}_{dopa-off}$ were the values of the post-operative and pre-operative scores without medication respectively, S^{post}_{score} and S^{pre}_{score} were the values of the post-operative and pre-operative neuropsychological scores respectively, $S_{\max}$ and $S_{\min}$ were the maximum and minimum on the score scale, respectively.

The surgical procedure consisted first, in attachment to the patient's head of a stereotactic Leksell frame, under local anaesthesia, then the implantation of bilateral quadripolar DBS electrodes (3387 Medtronic, Minneapolis, MN, USA) in the postero-ventral part of the two GPm in a single operating session [56]. Anti-parkinsonian treatment was stopped the evening before surgery. The patient was awake throughout the procedure and the effect of stimulation on rigidity was assessed by passive movement of the controlateral wrist. Programmable pulse generators (Medtronic) were implanted in the subclavicular region and connected to the electrodes.

Imaging data and electrode contact localization

All patients had one pre-operative 3-T T1-weighted MR (1 mm x 1 mm x 1 mm, Philips Medical Systems) and two CT scans (0.44 mm x 0.44 mm x 0.6 mm in post-operative acquisition and 0.5 mm x 0.5 mm x 0.6 mm in pre-operative acquisition, GE Healthcare VCT 64). Pre-operative scans were acquired after attachment to the patient's head of a stereotactic Leksell frame, under local anaesthesia. All images were de-noised using the non-local means algorithm [24] and a bias correction algorithm based on intensity values [72] was also applied to MR images.

We assembled information acquired from a population of patients onto one spatially normalized reference image (i.e. template). As a common space, we chose a multi-subject MR template created from a population of patients with PD (named the Parkinson template), with the segmentation of the basal ganglia and deep brain structures validated by a previous study [42] (Figure 1). After a preliminary step of automatic electrode contact segmentation based on image processing operations, combinations of linear and non-linear registrations allowed each stimulated contact to be warped in the Parkinson template. Both the contact segmentation and the registration algorithms were already meticulously and successfully validated [59]. Briefly, the registration workflow was composed of a linear CT to MRI registration, a global affine MR-to-template transformation, a local affine MR-to-template transformation with a mask on deep structures, and a final non-linear registration. Using this procedure the contact positions could be precisely warped into the MR template (Figure 1).

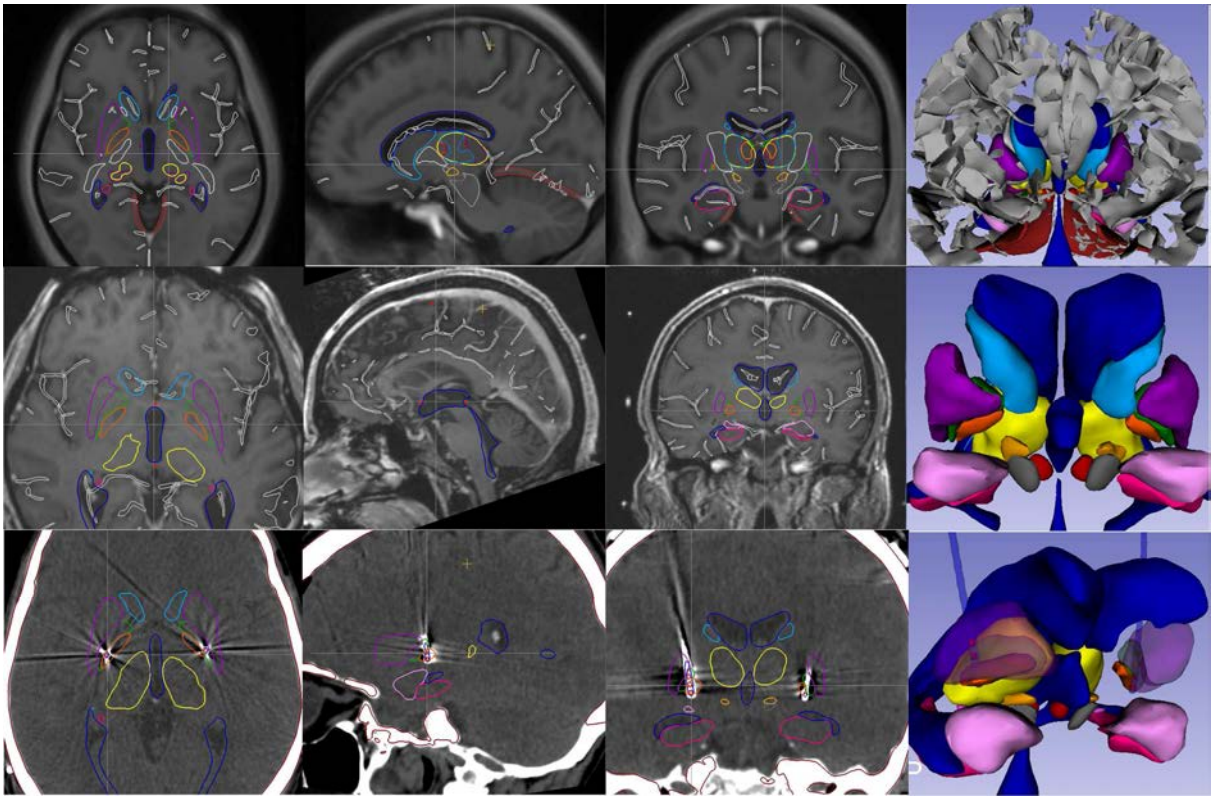

Figure 1. Axial, parasagittal, coronal and 3D views of 1) *first row*, the Parkinson template and the deep brain structure segmentation, 2) *second row*, a patient MRI with the registration of the deep brain structure segmentation on his MRI, and 3) *third row*, the postoperative CT with the registration of the deep brain structure segmentation, showing the location of the bilateral implanted electrodes in the GPm.

Amygdala (*light pink*), hippocampus (*dark pink*), putamen (*violet*), GPm (*orange*), lateral pallidum (*green*), caudate nucleus (*light blue*), thalami (*yellow*), substantia nigra (*grey*), STN (*light orange*), red nucleus (*red*), ventricles (*dark blue*).

Modeling of stimulation

Several methods have been proposed to model the electric field during DBS. In Guo et al. [40] and D'Haese et al. [29], a 3D Gaussian was simply used to approximate the electric field, then improved by the use of an annulus kernel in Pallavaram et al. [84]. For modeling the neural response, the activating function was used in Butson et al. [17] who proposed a modeling based on finite element model. At our site, mono-polar stimulation is generally proposed. Regarding the recent conclusion of Butson et al. [17] on the complexity of correctly simulating the stimulation phenomena, we decided to model the electric field using a single pre-defined 3D Gaussian. The parameters of the electrodes were: Medtronic® 3387 (4

contacts per electrode, 1.27 mm diameter, 1.5mm length) used with a monopolar stimulation protocol. In general, only one contact per electrode was stimulated, except for certain GPm patients. Based on these parameters and on the quasi-static potential equation, the stimulation influence covers approximately a 3 mm-radius sphere around each stimulation contact.

Statistical maps

The idea was to create general maps that could easily be read and interpreted by clinicians. Statistical maps should take into account the number of patients, the stimulation zone for each patient, as well as all responses to clinical testing of each patient. Therefore, the value at a given voxel is an average of clinical scores of patients that have active contacts in the same area, weighted by the distance to the active patient contact. Using such a definition eliminates the need to define inclusion criteria and the value at a given voxel does not represent a probability but a global efficacy score. In order to take into account the statistical meaningfulness at a given voxel, we also propose 'Patient Maps' indicating the number of patients participating in the computation of the final weighted voxel value. At each voxel of a 'Statistical Map' for a given score, the computation of the final value has been made using between one to 20 patients. A color code was used to represent how many patients were used for a given statistical map.

Results

Stimulation contact and parameters

Given the size of the GPm, 6 patients were stimulated on two contacts, 0 and 1 or 1 and 2 bilaterally with monopolar stimulation. One patient had contacts 0 and 1 stimulated on the right side and contact 0 stimulated on the left side. The 13 other patients had only one contact stimulated bilaterally. Six months after surgery, the mean position of the active electrode's contacts was calculated by making first, an average of the coordinates in each patient with double stimulated contacts, and secondly, an average of all the coordinates in all the patients. The mean coordinates of the active contact was:

- on the left side: 23.9 ±1.9 mm for the lateral direction, 7.9 ±2.3 mm posterior to the anterior commissure, and 2.9 ±2.9 mm under the AC-PC line for the dorso-caudal direction;
- on the right side: 23.5 ±2 mm for the lateral direction, 8.1 ±2.4 mm posterior to the anterior commissure, 2.77 ±3.5 mm under the AC-PC line for the dorso-caudal direction.

The average stimulation parameters were:

- on the left side, a voltage of 2.76 ±0.4 V, pulse frequency of 135 ±122 Hz, pulse amplitude of 77.3 ±23 μs
- on the right side, a voltage of 2.76 ±0.4 V, pulse frequency of 133 ±11.8 Hz, pulse amplitude of 72.6 ±15.2 μs.

Statistical maps

We obtained two maps per score, the first one (the 'Statistical Map') representing the change of the score per voxel, by a color scale from blue to red, and the second one (the 'Patient Map') representing the number of patients per voxel used for the final score computation. The ‘Patient Map’ was also coded using a color scale from blue (one patient) to red (highest number of patients). For instance, a dark red point on the ‘Statistical Map’ would represent only one or two patients on the 'Patient Map” whereas another orange voxel zone on the ‘Statistical Map’ would represent ten patients on the ‘Patient Map’ and would be more representative of the patient group. For the UPDRS III, the color scale was reversed: dark red (deterioration) to dark blue (improvement) because of the negativity of the score *S%*. For the other scores, the color scale was dark blue (deterioration) to dark red (improvement).

- For the UPDRS III, we obtained a 'Patient Map' (Figure 2, *bottom row*, red points) showing most of the patients stimulated in the postero-ventral part of the GPm on the right side and in the postero-ventral and more lateral part of the GPm on the left side. For these regions, the UPDRS III was represented in blue to orange colors (Figure 2, *top row*), meaning an *S%* score between -0.2 to -0.12 (Table 1), therefore an improvement of the postoperative score.

TABLE 1. Scores of patients with GPm DBS: details of scores and number of patients for 'Statistical' and 'Patient' maps.

Scores ***S%***	**Total Number of Patients**	**Min-Max of the score**	**'Patients Map': voxels with a maximum of patients**	**'Stat Map': Scores at the max number of patients**
UPDRS III	20	-0.62 / 0.11	7	-0.2 / -0.12
MDRS	20	-0.03 / 0.08	7	0.001 / 0.03
Phonemic Fluency	19	-0.33 / 0.26	6	-0.12 / -0.05
Categorical Fluency	19	-0.5 / 0.23	7	-0.11 / 0.15
Stroop test	20	-0.37 / 0.66	7	0.03 / 0.13

4th column shows the maximum number of patients in the red zone in the 'Patients map'.
The Last column shows the scores in the regions of the 'Statistical Map', corresponding to the regions of the red points on the 'Patients Map'.
MDRS, Mattis dementia rating score; Max, maximum; Min, minimum; Stat Map, Statistical map; UPDRS, Unified Parkinson's Disease Rating Scale.

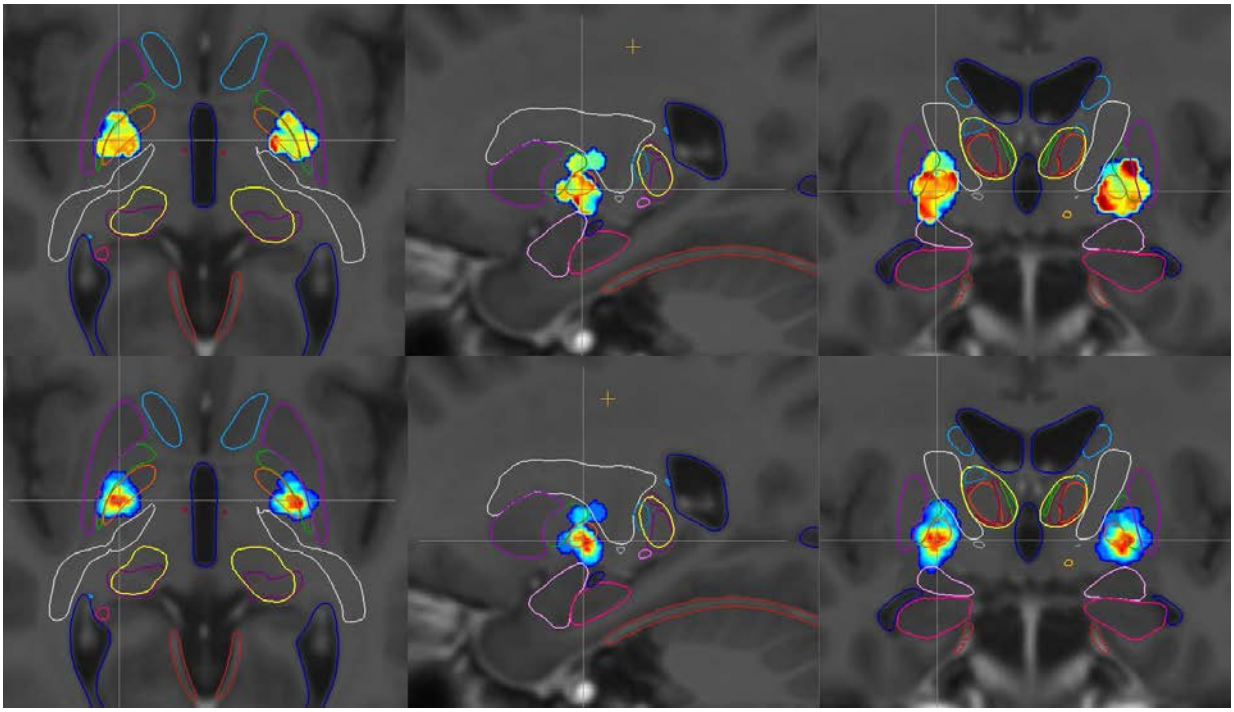

Figure 2. Axial, sagittal and coronal views of the Parkinson template showing the 'Statistical Map' *(top)* and the 'Patients Map' *(bottom)* built on **UPDRS III analysis** in 20 patients with GPm DBS at 6 months postoperatively.

- For the Hoehn and Yahr and the Schwab and England scales, the 'Statistical Maps' were relatively homogeneous at 6 months post-operatively, showing a stability of these scores compared to the preoperative state.

- For the MDRS, most of the patients were stimulated in the same places as for the UPDRS III (Figure 3, *bottom row*). In these locations, the MDRS did not vary post-operatively and was represented in blue in the postero-ventral part of the GPm on the 'Statistical Map' (Figure 3, *top row*). The *S%* scores were between 0.001 and 0.03 in the regions of the 'Statistical Map', corresponding to the red points on the 'Patients Map' (Table 1).

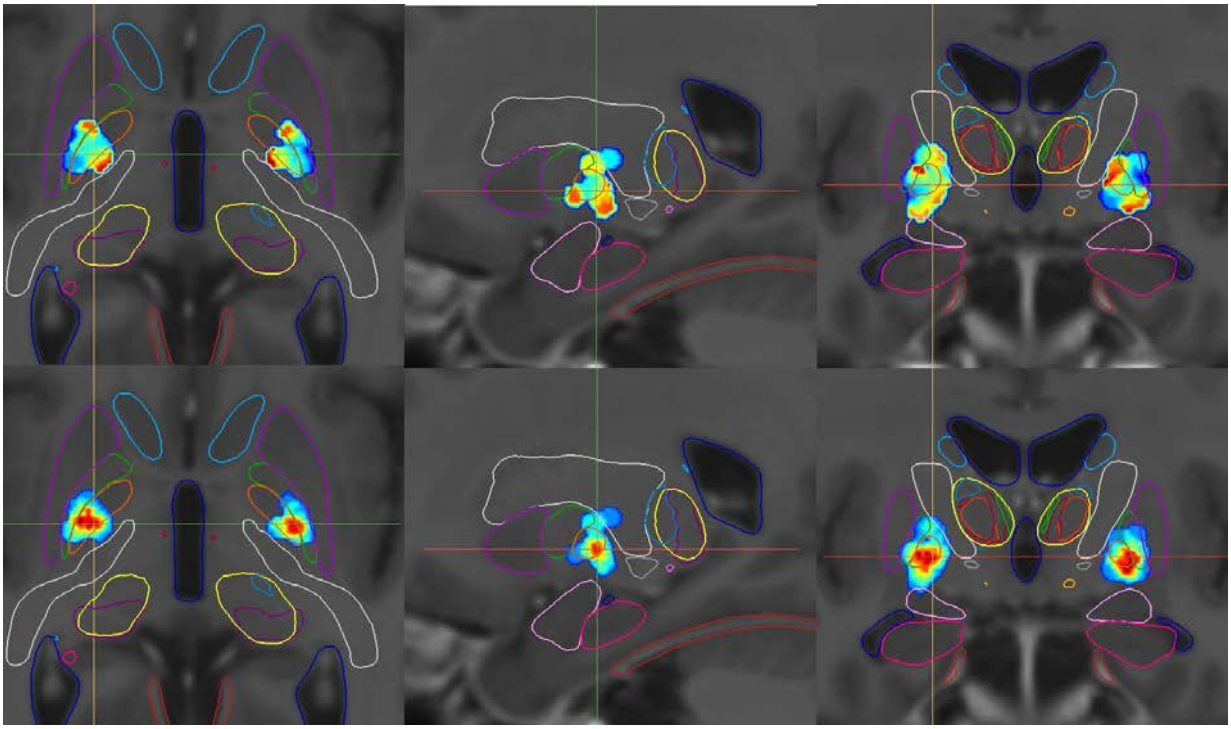

Figure 3. Axial, sagittal and coronal views of the Parkinson template showing the 'Statistical Map' (*top*) and the 'Patients Map' (*bottom*) built on **MDRS analysis** in 20 patients with GPm DBS at 6 months postoperatively.

- <u>For the phonemic fluency</u>, we analyzed only 19 patients and the majority of these were stimulated in the same places as for the UPDRS III (Figure 4, *bottom row*). For these locations, phonemic fluency was represented in blue on the right side and in orange on the left side on the 'Statistical Maps' (Figure 4, *top row*). The *S%* scores were between -0.05 and -0.12 in the regions of the 'Statistical Map', corresponding to the red points on the 'Patients Map' (Table 1).

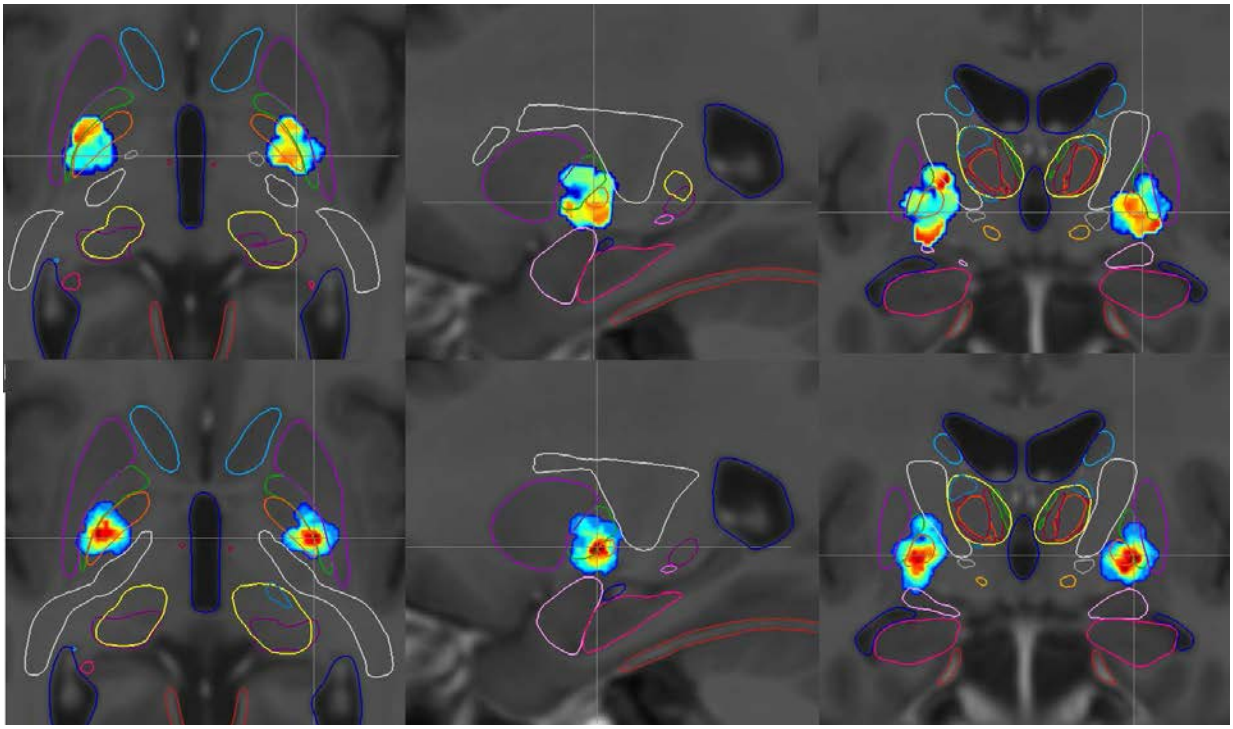

Figure 4. Axial, sagittal and coronal views of the Parkinson template showing the 'Statistical Map' (*top*) and the 'Patients Map' (*bottom*) built on **phonemic fluency** analysis in 20 patients with GPm DBS at 6 months postoperatively.

- For the categorical fluency, we analyzed only 19 patients and most of these were stimulated in the same places as for the UPDRS III (Figure 5, *bottom row*). For these locations, categorical fluency was represented in orange-red on the right side and in yellow-orange on the left on the 'Statistical Maps' (Figure 5, *top row*). The *S%* scores were between -0.11 and 0.15 in the regions of the 'Statistical Map', corresponding to the red points on the 'Patients Map' (Table 1).

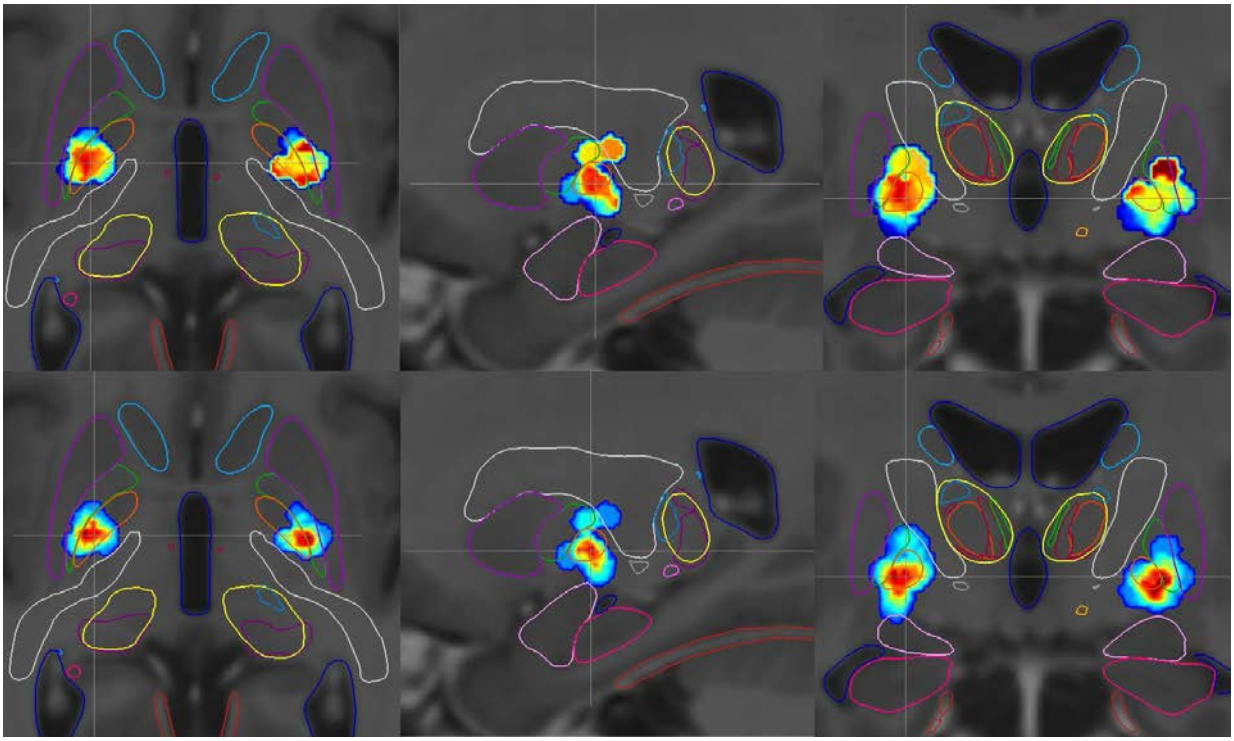

Figure 5. Axial, sagittal and coronal views of the Parkinson template showing the 'Statistical Map' (*top*) and the 'Patients Map' (*bottom*) built on **categorical fluency** analysis in 20 patients with GPm DBS at 6 months postoperatively.

- For the Stroop test, most patients were stimulated in the same places as for the UPDRS III (Figure 6, *bottom row*). For these locations, categorical fluency was represented in blue on both sides of the 'Statistical Maps' (Figure 6, *top row*). The *S%* scores were between 0.03 and 0.13 in the regions of the 'Statistical Map', corresponding to the red points on the 'Patients Map' (Table 1).

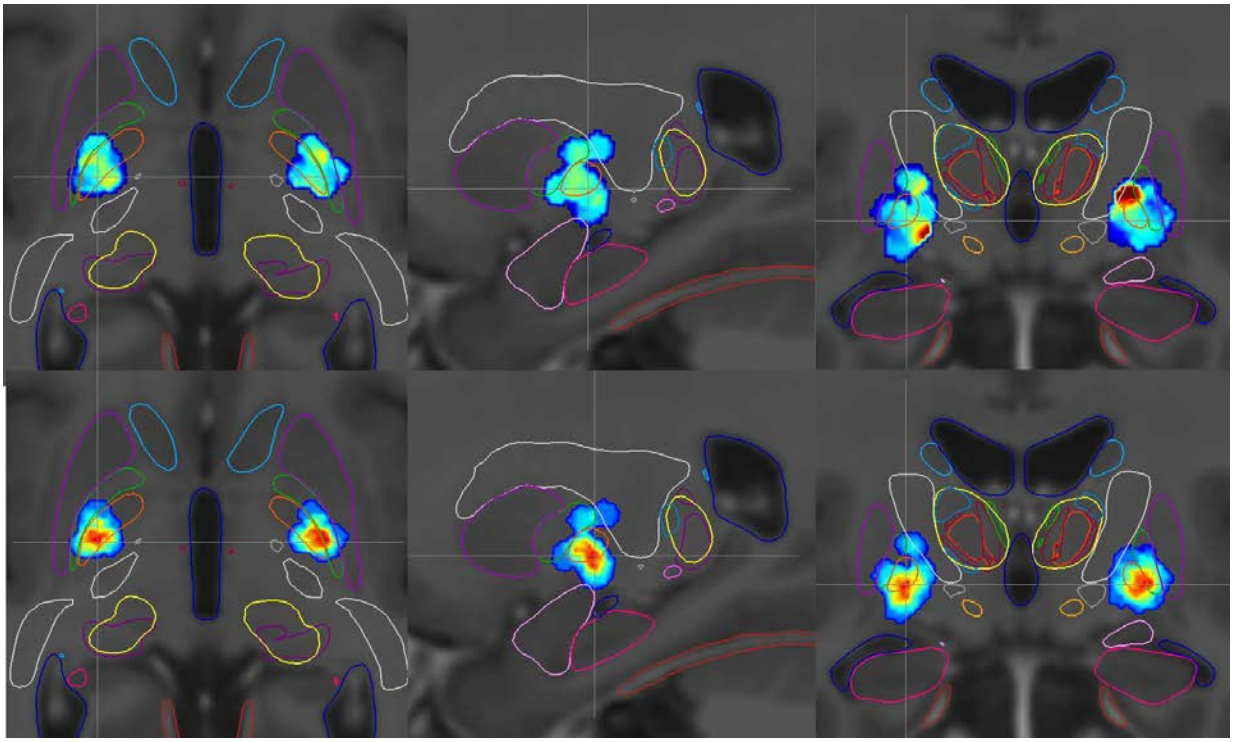

Figure 6. Axial, sagittal and coronal views of the Parkinson template showing the 'Statistical Map' (*top*) and the 'Patients Map' (*bottom*) built on **Stroop test analysis** in 20 patients with GPm DBS at 6 months postoperatively.

Discussion

To our knowledge, this article is the first report on the construction of anatomo-clinical 3D maps in patients with GPm stimulation and severely disabled Parkinson's disease. We observed the motor improvement of such patients by stimulating the postero-ventral part of the GPm. The efficacy of GPm stimulation in Parkinson's disease has often been demonstrated in the literature [35,94,108,109]. However the choice between STN and GPm DBS is still under debate. In our opinion and in accordance with our experience, these two targets should not be chosen in the same patients. Classically, the STN DBS is the appropriate DBS for patients without cognitive impairments and/or dopa-resistant axial motor symptoms (dysarthria, freezing, and/or falls) whereas the GPm DBS can be proposed to such disabled patients when they have also dopa-induced dyskinesias. A limit is a severe cortico-subcortical atrophy on preoperative MRI which contra-indicates the surgery.

We built the anatomo-clinical 3D maps within a common spatial referential, the Parkinson Template, by automatically detecting the contacts of the electrodes on the postoperative CT and by using a validated registration tool to obtain a reliable localization of the clinical and anatomical data on the Parkinson template. Some limits to our method were 1) the use of different registration steps to obtain volume of stimulation on the Parkinson template, 2) the estimation of the stimulation volume by a 3mm Gaussian around the stimulated contacts and 3) the arbitrary color coding of the *S%*. Concerning the registration tools, we have already published the comparison between 3 registration tools and the validation of each tool in terms of registration errors [42,59]. The registration approach used in this paper was the most accurate, combined with the use of a multi-subject rather than a mono-subject template [59]. Our choice for modeling the neural response to stimulation was based on the current state of reflection carried out by Butson et al. [17]. The authors, regarding their long time-consuming processing of a stimulation model, proposed an online tool easier to use in our case [17]. We need further studies on the modeling of a clinical score by color scale to render it more informative for clinicians. Our goal was to use the 'Statistical and Patient Maps' in clinical practice of DBS, without needing engineer time. Nevertheless, the statistical maps remain today a 3D tool more easily readable on a computer than on 2D.

We developed these ‘Statistical maps’ into a specific DBS software package (PyDBS) and began to use it in clinical practice while waiting for its clinical validation.

Concerning the neuropsychological consequences of STN DBS, we have already published anatomo-clinical atlases for 30 patients operated on for STN DBS [59]. These first anatomo-clinical atlases did not take into account the volume of stimulation and we did not have the registration of the atlases on the template to visualize accurately the STN and the adjacent structures. We demonstrated a discrepancy between a good motor improvement of the STN DBS in the postero-lateral part of the STN and an impairment of the fluencies in the same region. Now the ‘Statistical Maps’ provided us with a more accurate and realistic effect of the stimulation in the GPm, the lateral pallidum and the adjacent structures. We obtained similar results to those previously published in the literature [94] about the motor improvement of GPm stimulation patients and a global stability of neuropsychological scores after GPm stimulation. More accurately, we observed at 6 months a stability of the MDRS, stability and even for some patients slight improvement in the Stroop test, and a degradation of phonemic fluency whatever the location in the GPm, whereas categorical fluency showed a tendency to decrease or improve according to the patient. This point is important in patients with preoperative cognitive impairment. We even showed a slight improvement in the Stroop test that could be an interesting therapeutic point in such disabled patients.

According to the Talairach atlas [103], our target was 23.9 mm to the left and 23.5 mm to the right, 8 mm on average posterior to the anterior commissure and almost 3 mm under the AC-PC line. According to Laitinen et al. [55,56] and Schaltenbrand atlas [97], the GPm targeting was described as 2 to 3 mm anterior to the mid-commissural point between AC and PC, 18 to 22 mm lateral and 6 to 7 mm below the intercommissural line. In our study, the average contact was located more laterally perhaps due to a large third ventricle because of severe cortico-subcortical atrophy induced by the PD. An article [65] even reported direct GPm targeting for 5 PD patients 15.3 mm laterally, 9 mm anterior to the midpoint and 1.4 to 1.7 mm under the AC-PC line. These authors reported a statistical motor improvement of the patients at 6 months but they did not publish either neuropsychological or psychiatric analysis. [65]. Their targeting was probably anterior, in the more central part of the GPm, which, in

anatomical studies, projects to the centro-median nucleus [83] and the lateral habenular nucleus [86,87], both being part of the limbic system. The pallidum is not directly connected to the cortex and has its major efferent projections to the motor thalamic nuclei, namely the ventral anterior and lateral nuclei, via the ansa lenticularis and lenticular fasciculus. Through the indirect pathway of the cortico-striato-pallido-thalamo-cortical motor circuit, the lateral pallidum projects to the STN [1,11,87]. By its well-defined and closed afferent and efferent connections, the postero-ventral part of the GPm essentially has a sensori-motor role, as does the lateral pallidum [93]. Both the sensori-motor territories of the lateral pallidum and GPm have a somatotopic organization characterized by a leg region mediodorsal to the arm and face regions.

Perhaps the GPM stimulation has neuropsychological and psychiatric effects due its well separated connections to the motor and limbic circuits of the basal ganglia, and due to its quasi-absence of direct cortical connections at the difference with the STN. Pallidotomy produced marked motor improvement in PD patients without their experiencing cognitive deterioration according to the lesion location [68]. More anterior lesions affecting the limbic part of the GPm led to postoperative cognitive deterioration [68], not seen in a meta-analysis of patient outcome after GPm stimulation [35,108]. Inside the motor parts of the lateral pallidum and GPm, Yelnik et al. [111] described different effects of the stimulation on the motor symptoms. They observed that rigidity was improved whatever the site of stimulation in the motor pallidum whereas akinesia was improved only by stimulating the lateral pallidum. The site where the akinesia was worst in the motor GPm was also the site which improved dopamine-induced dyskinesia. Their contacts which stimulated the lateral pallidum were those dorsal on the electrode and the contacts stimulating the GPm were those ventral. In our study, most of the patients were stimulated at the junction between the GPm and the lateral pallidum, especially visible on the left side of the ‘Patients maps’. The GPm being larger than the STN, GPm stimulation sometimes needs to stimulate two contacts thus potentially mixing motor improvements on akinesia, rigidity and dopamine-induced dyskinesia.

Conclusions

As a conclusion, we developed new statistical anatomo-clinical maps the better to visualize the motor and neuropsychological consequences at 6 months of GPm stimulation in patients with PD. These maps provided us with the confirmation of the motor improvement of GPm stimulation without cognitive impairments. We also proposed a new more lateral targeting of the GPm in PD because of the cortico-subcortical atrophy induced by the disease. Our goal is to use these ‘Statistical Maps’ prospectively in further patients to improve their targeting, thus ensuring a shorter planning step on the day of the surgery as well as better outcomes from motor and neuropsychological point of view.

CONCLUSIONS

Conclusions

The different steps of the construction and validation of a multimodal database was:

- *The construction of a multi-subject MRI template specific to patients with Parkinson's disease*

From the Parkinson template, we segmented the basal ganglia and deep brain structures such as the hippocampus and the amygdala. We compared three methods of automatic segmentation to validate the segmentation of the Parkinson template. We noticed little difference between the methods in terms of their accuracy but differences in terms of processing time. A novel method named "the patch-based label fusion method" was the fastest, but still needed engineer processing and is not usable in clinical practice.

- *The use of the Parkinson template segmentation in patients*

We analysed the results of two registration tools in terms of registration accuracy and showed that the SyN tool [50] was the most accurate. We decided to transform all the patients' imaging data into the Parkinson template using this tool, and in particular the location of the electrode contacts in the basal ganglia. This validation step was the second step of the construction of our multimodal database to be used it hereafter in clinical practice to obtain the segmentation of the basal ganglia in a new patient MRI.

- *Postoperative results analysis of 30 patients stimulated in the STN*

We built anatomo-clinical atlases of one motor and three neuropsychological scores by using a non-supervised statistical tool, a Hierarchical Ascendant Classification. We obtained different results in agreement with the data in the literature and a new explanation of neuropsychological impairment observed after STN stimulation. We showed a discrepancy between good motor improvement when targeting the postero-superior region of the STN and inevitable deterioration of categorical and phonemic fluency in the same region. This third step was a first approach to correlate anatomical with clinical data without an a priori hypothesis.

- *Postoperative results analysis of 20 patients stimulated in the GPm*

To improve the previous analysis, we built new statistical maps to better take into account both the volume of stimulation instead of a point representing the electrode contact, and the number of patients receiving a given stimulation volume. We obtained 'Statistical Maps' representing the postoperative evolution of a score by a color scale, and 'Patient Maps' defining exactly how many patients were represented in a given voxel. The two maps were observed on the basal ganglia segmentation of the Parkinson template. The goal was to build maps useful for a neurosurgeon before implantation of a new patient. We demonstrated good motor improvement without severe neuropsychological deterioration after GPm stimulation. Our targeting was more lateral than those previously described in the literature, probably due to the brain atrophy of severely disabled patients.

These studies illustrated the different validation steps of a multimodal database construction on Parkinsonian patients before its use it in clinical practice. This allows us to be sure of the following steps:

- Registration of the Parkinson template segmentation on the patients imaging
- Visualization of the basal ganglia on the patient MRI to optimize its targeting
- Optimization of new targeting by analysis of postoperative results, whether motor or neuropsychological.

Study perspectives

1) The purpose is to use the multimodal database in DBS clinical practice according to three distinct steps:

- First, an inclusion step with the preoperative MRI, in which an automatic cutaneous and brain segmentation is made as a registration of the Parkinson template segmentation on the MRI, and as a manual AC and PC detection on the MRI;
- Second, a preoperative step with the preoperative CT acquired with the frame, in which the frame is automatically recognized and the CT registered to the preoperative MRI;
- Third, a postoperative step, with the postoperative CT, in which the electrode contacts are automatically recognized.

Our purpose is to develop an integrated and fully automated processing pipeline, named PyDBS, to be used as a toll to assist accurate targeting and to analyse postoperative results. To validate PyDBS, we will need prospective analysis of new implanted patients to compare the postoperative clinical results and the differences in the surgical practice such as the duration of the surgery. A secondary objective will be a shorter and more comfortable surgery time for the patient.

2) The purpose of the Statistical Maps is to develop new analysis in other diseases:

- for 10 patients with GPm stimulation for Tourette's syndrome;
- for 40 patients with VLc stimulation for PD and/or essential tremor.

These analyzes will provide us with new clinical information and consequences of the DBS in targets less studied than the STN.

3) With the segmentation of deep brain structures and of the different thalamic nuclei, PyDBS would be applied in DBS in epilepsy, especially in the project of anterior thalamic nucleus stimulation in pharmaco-resistant epileptic patients in France.

References

1- Alexander GE, DeLong MR, Strick PL. Parallel organization of functionally segregated circuits linking basal ganglia and cortex. **Ann Rev Neurosci 9:**357-81, 1986

2- Aljabar P, Heckeman RA, Hammers A, Hajnal JV, Rueckert D. Multi-atlas based segmentation of brain images: atlas selection and its effect on accuracy. **Neuroimage 46:**726-38, 2009

3- Antonini A, Isaias IU, Rodolfi G, Landi A, Natuzzi F, Siri C, Pezzoli G. A 5-year prospective assessment of advanced Parkinson disease patients treated with subcutaneous apomorphine infusion or deep brain stimulation. **J Neurol 258**:579-85, 2011

4- Aubert-Broche B, Evans AC, Collins L. A new improved version of the realistic digital brain phantom. **Neuroimage 32:**138-45, 2006

5- Avants BB, Epstein CL, Grossman M, Gee JC. Symmetric diffeomorphic image registration with cross-correlation: evaluating automated labeling of elderly and neurodegenerative brain. **Med Image Anal 12(1)**:26-41, 2008

6- Bardinet E, Dormont D, Malandain G, Bhattachargee M, Pidoux B, Saleh C, Cornu P, Ayache N, Agid Y, Yelnik J. Retrospective cross-evaluation of an histological and deformable 3D atlas of the basal ganglia on series of Parkinsonian patients treated by deep brain stimulation. **LNCS MICCAI**, Springer-Verlag, 3750:385-93, doi: 10.11007/11566489_48, 2005

7- Bardinet E, Bhatttacharjee M, Dormont D, et al. A three-dimensional histological atlas of the human basal ganglia.II. Atlas deformation strategy and evaluation in deep brain stimulation for Parkinson disease. **J Neurosurg 110:**208-19, 2009

8- Benabid AL, Krack P, Benazzouz A, Limousin P, Koudsie A, Pollak P. Deep brain stimulation of the subthalamic nucleus for Parkinson's disease: methodologic aspects and clinical criteria. **Neurology 55:** 40-4, 2000

9- Benabid AL, Koudsié A, Benazzouz A, Fraix V, Ashraf A, Le Bas JF, Chabardes S, Pollak P. Subthalamic stimulation for Parkinson's disease. **Arch Med Res 31:**282-9, 2000

10- Benabid AL, Chabardes S, Mitrofanis J, Pollak P. Deep brain stimulation of the subthalamic nucleus for the treatment of Parkinson's disease. **Lancet Neurol 8:**67-81, 2009

11- Bergman H, Wichmann T, Karmon B, DeLong MR. The primate subthalamic nucleus. II. Neuronal activity in the MPTP model of parkinsonism. **J Neurophysiol 72(2):**507-20, 1994

12- Bhattachargee M, Pitiot A, Roche A, Dormont D, Bardinet E. Anatomy-preserving nonlinear registration of deep brain ROIs using confidence-based block-matching. **LNCS MICCAI**, part II, Springer-Verlag, 5242:956-63, doi: 10.1007/978-3-540-85990-1_115, 2008

13- Biseul I, Sauleau P, Haegelen C, et al. Fear recognition is impaired by subthalamic nucleus stimulation in Parkinson's disease. **Neuropsychologia 43**:1054-9, 2005

14- Brontë-Stewart H, Louie S, Batya S, Henderson JM. Clinical motor outcome of bilateral subthalamic nucleus deep-brain stimulation for Parkinson's disease using image-guided frameless stereotaxy. **Neurosurgery 67(4):**1088-93, 2010

15- Brücke C, Kupsch A, Schneider GH, et al. The subthalamic region is activated during valence-related emotional processing in patients with Parkinson's disease. **Eur J Neurosci 26:**767-74, 2007

16- Burrows AM, Ravin PD, Novak P, Peters ML, Dessureau B, Swearer J, Pilitsis JG. Limbic and motor function comparison of deep brain stimulation of the zona incerta and subthalamic nucleus. **Neurosurgery 70(1):**125-30, 2011

17- Butson CR, Cooper SE, Henderson JM, Wolgamuth B, McIntyre CC. Probabilistic analysis of activation volumes generated during deep brain stimulation. **Neuroimage 54:**2096-104, 2011

18- Cardebat D, Doyon B, Puel M, Goulet P, Joanette Y. Evocation lexicale formelle et sémantique chez des sujets normaux: performances et dynamiques de production en fonction du sexe, de l'âge et du niveau d'étude. **Acta Neurol Belg 90:**207–17, 1990

19- Chakravarty M, Bertrand G, Hodge CP, Sadikot AF, Collins DL. The creation of a brain atlas for image guided neurosurgery using serial histological data. **Neuroimage 30(2):**359-76, 2006

20- Chakravarty MM, Sadikot AF, Germann J, Hellier P, Bertrand G, Collins DL. Comparison of piece-wise linear, linear, and nonlinear atlas-to-patient warping techniques: analysis of the labelling of subcortical nuclei for functional neurosurgical applications. **Hum Brain Mapp 30:**3574-95, 2009

21- Collins DL, Neelin P, Peters TM, Evans AC. Automatic 3D intersubject registration of MR volumetric data in standardized Talairach space. **J Comput Assist Tomogr 18:**192-205, 1994

22- Collins DL, Holmes CJ, Peters T, Evans AC. Automatic 3-D model based neuoranatomical segmentation. **Hum Brain Mapp 3**:190-208, 1995

23- Collins DL, Pruessner JC. Towards accurate, automatic segmentation of the hippocampus and amygdala from MRI by augmenting ANIMAL with a template library and label fusion. **Neuroimage 52:**1355-66, 2010

24- Coupé P, Yger P, Prima S, Hellier P, Kervrann C, Barillot C. An optimized blockwise nonlocal means denoising filter for 3-D magnetic resonance images. **IEEE TMI 24**:425-41, 2008

25- Coupé P, Manjon JV, Fonov V, Pruessner J, Robles M, Collins DL. Patch-based segmentation using expert priors: application to hippocampus and ventricle segmentation. **Neuroimage 54:**940-54, 2011

26- Dawant B, D'Haese PF, Pallavaram S, Li R, Yu H, Spooner J, Davis T, Kao C, Konrad P. The VU-DBS project: integrated and computer-assisted planning, intra-operative placement, and post-operative programming of deep-brain stimulators. **SPIE Medical Imaging 6509(1):**650907, 2007

27- D'Haese PF, Cetinkaya E, Konrad PE, Kao C, Dawant BM. Computer-aided placement of deep brain stimulators: From planning to intraoperative. **IEEE TMI 24(11)**:1469-78, 2005

28- D'Haese PF, Pallavaran S, Yu H, Spooner J, Konrad PE, Dawant BM. Deformable physiological atlas based programming of deep brain stimulators: a feasability study. WBIR, Utrecht, The Netherlands 144-50, 2006

29- D'Haese PF, Pallavaram S, Li R, Remple MS, Kao C, Neimat JS, Konrad PE, Dawant BM. CranialVault and its CRAVE tools: A clinical computer assistance system for deep brain stimulation (DBS) therapy. **Med Image Anal 16:** 744-53, 2012

30- Dice L. Measure of the amount of ecological association between species. **Ecology 26(3):**297–302, 1945

31- Dormont D, Seidenwurm D, Galanaud D, Cornu P, Yelnik J, Bardinet E. Neuroimaging and deep brain stimulation. **AJNR 31(1):**15-23, 2010

32- Dujardin K., Blairy S, Defebvre L, Krystkowiak P, Hess U, Blond S, Destee A. Subthalamic nucleus stimulation induces deficits in decoding emotional facial expressions in Parkinson's disease. **J Neurol Neurosurg Psychiatry 75:**202-8, 2004

33- Fahn S, Elton R, UPDRS Development Committee: Unified Parkinson's disease rating scale, in Fahn S, Marsden CD, Calne DB, et al (eds). Recent Developments in Parkinson's Disease. Florham Park, NJ: Macmillan, pp 153-63, 1987

34- Finnis KW, Starreveld YP, Parrent AG, Sadikot AF, Peters TM. Three-dimensional database of subcortical electrophysiology for image-guided stereotactic functional neurosurgery. **IEEE Trans Med Imaging 22(1):**93-104, 2003

35- Follett K, Weaver F, Stern M, et al. Pallidal versus subthalamic deep-brain stimulation for Parkinson's disease. **N Engl J Med 362**: 2077-91, 2010

36- Fonov V, Evans AC, Botteron K, Almli CR, McKinstry RC, Collins DL, Brain Development Cooperative Group. Unbiased average age-appropriate atlases for pediatric studies. **Neuroimage 54:**313-27, 2011

37- Gibb WR, Lees AJ. The relevance of the Lewy body to the pathogenesis of idiopathic Parkinson's disease. **J Neurol Neurosurg Psychiatry 51:** 745-52, 1998

38- Greenhouse I, Gould S, Houser M, Hicks G, Gross J, Aron AR. Stimulation at dorsal and ventral electrode contacts targeted at the subthalamic nucleus has different effects on motor and emotion functions in Parkinson's disease. **Neuropsychologia 49:**528-34, 2011

39- Guehl D, Edwards R, Cuny E, Burbaud P, Rougier A, Modolo J, Beuter A. Statistical determination of the optimal subthalamic nucleus stimulation site in patients with Parkinson disease. **J Neurosurgery 106:**101-10, 2007

40- Guo T, Finnis KW, Parrent AG, Peters TM. Visualization and navigation system development and application for stereotactic deep-brain neurosurgeries. **Comput Aided Surg 11:**231-39, 2006

41- Guo T, Parrent AG, Peters TM. Surgical targeting accuracy analysis of six methods for subthalamic nucleus deep brain stimulation. **Comput Aided Surg 12:**325-34, 2007

42- Haegelen C, Coupe P, Fonov V, Guizard N, Jannin P, Morandi X, Collins DL. Automated segmentation of basal ganglia and deep brain structures in MRI of Parkinson's Disease. **Int J Comput Assist Radiol Surg 8:** 99-110, 2013

43- Hamani C, Saint-Cyr JA, Fraser J, Kaplitt M, Lozano AM. The subthalamic nucleus in the context of movement disorders. **Brain 127(1):**4-20, 2003

44- Hoehn M, Yahr M. Parkinsonism: onset, progression and mortality. **Neurology 17:**427-442, 1967

45- Houeto JL, Mesnage V, Mallet L, et al. Behavioural disorders, Parkinson's disease and subthalamic stimulation. **J Neurol Neurosurg Psychiatry 72:**701-7, 2002

46- Hu S, Coupé P, Pruessner JC, Collins DL. Appearance-based modeling for segmentation of hippocampus and amygdala using multi-contrast MR imaging. **Neuroimage 58:**549-59, 2011

47- Karachi C, Yelnik J, Tandé D, Tremblay L, Hirsch E, François C. The pallidosubthalamic projection: An anatomical substrate for nonmotor functions of the subthalamic nucleus in primates. **Mov Disord 20(2):**172-80, 2005

48- Khan MF, Mewes K., Gross RE, Skrinjar O. Assessment of brain shift related to deep brain stimulation surgery. **Stereotact Funct Neurosurg 86(1):**44-53, 2008

49- Kim YH, Kim HJ, Kim C, Kim DG, Jeon BS, Paek SH. Comparison of electrode location between immediate postoperative day and 6 months after bilateral subthalamic nucleus deep brain stimulation. **Acta Neurochirurgica 152(12):**2037-45, 2010

50- Klein A, Andersson J, Ardekani BA, et al. Evaluation of 14 nonlinear deformation algorithms applied to human brain MRI registration. **Neuroimage 46:**786-802, 2009

51- Koller W, Pahwa R, Lyons K, Wilkinson S. Deep brain stimulation of the Vim nucleus of the thalamus for the treatment of tremor. **Neurology 55:**S29-S33, 2000

52- Krack P, Pollak P, Limousin P, Hoffmann D, Xie J, Benazzouz A, Benabid AL. Subthalamic nucleus or internal pallidal stimulation in Young onset Parkinson’s disease. **Brain 121:**451-7, 1998

53- Krack P, Batir A, Van Blercom N, et al. Five-year follow-up of bilateral stimulation of the subthalamic nucleus in advanced Parkinson’s disease. **N Engl J Med 349:**1925-34, 2003

54- Kühn AA, Hariz MI, Silberstein P, Tisch S, Kupsch A, Schneider GH, Limousin-Dowsey P, Yarrow K, Brown P. Activation of the subthalamic region during emotional processing in Parkinson disease. **Neurology 65:**707-13, 2005

55- Laitinen LV, Bergenheim AT, Haritz MI. Ventralposteromedial pallidotomy can abolish all Parkinsonian symptoms. **Stereotact Funct Neurosurg 58:**14-21, 1991

56- Laitinen LV, Bergenheim AT, Haritz MI. Leksell’s posteroventral pallidotomy in the treatment of Parkinson’s disease. **J Neurosurg 76:**53-61, 1992

57- Lalys F, Haegelen C, Abadie A, Jannin P. Post-operative assessment in deep brain stimulation based on multimodal images: registration workflow and validation. In Medical Imaging 2009: Visualization, Image-Guided Procedures, and Modelling

58- Lalys F, Haegelen C, Ferre JC, El-Ganaoui O, Jannin P. Construction and assessment of a 3T MRI brain template. **Neuroimage 49:**345-54, 2010

59- Lalys F, Haegelen C, Mehri M, Drapier S, Verin M, Jannin P. Anatomo-clinical atlases using clinical data and electrode contact coordinates: application to subthalamic deep brain stimulation. **J Neurosc Meth 212:**297-307, 2012

60- Lambert C, Zrinzo L, Nagy Z, Lutt, A, Hariz M, Foltynie T, Draganski B, Ashburner J, Frackowiak R. Confirmation of functional zones within the human subthalamic nucleus: patterns of connectivity and sub-parcellation using diffusion weighted imaging. **Neuroimage 60(1):**83-94, 2012

61- Lang AE, Lozano AM. Parkinson's Disease.**New Engl J Med 339**:1044-1053, 1998

62- Langston JW, Widner H, Goetz CG, Brooks D, Fahn S, Freeman T, Watts R. Core assessment program for intracerebral transplantation (CAPIT). **Mov Dis 7**:2-13, 1992

63- Lanotte MM, Rizzone M, Bergamasco B, Faccani G, Melcarne A, Lopiano L. Deep brain stimulation of the subthalamic nucleus: anatomical, neurophysiological, and outcome correlations with the effects of stimulation. **J Neurol Neurosurg Psychiatry 72:**53-8, 2002

64- Lee JY, Kim JW, Lee JY, Lim YH, Kim C, Kim DG, Jeon BS, Paek SH. Is MRI a reliable tool to locate the electrode after deep brain stimulation surgery? Comparison study of CT and MRI for the localization of electrodes after DBS. **Acta Neurochir 152(12):**2029-36, 2010

65- Lemaire JJ, Durif F, Boire JY, Debilly B, Irthum B, Chazal J. Direct stereotactic MRI location in the globus pallidus for chronic stimulation in Parkinson's disease. **Acta Neurochir (Wien)141:**759-66, 1999

66- Lenglet C, Abosch A, Yacoub E, De Martino F, Sapiro S, Harel N. Comprehensive in vivo mapping of the human basal ganglia and thalamic connectome in individuals using 7T MRI. **PLoS One 7(1):**e29153. doi: 10.1371/journal.pone.0029153, 2012

67- Lhommée E, Klinger H, Thobois S, et al. Subthalamic stimulation in Parkinson's disease: restoring the balance of motivated behaviours. **Brain 135:**1463-77, 2012

68- Lombardi WJ, Gross RE, Trepanier LL, Lang AE, Lozano AM, Saint-Cyr JA. Relationship of lesion location to cognitive outcome following microelectrode-guided pallidotomy for Parkinson's disease. **Brain 123:**746-58, 2000

69- Mai JK, Paxinos G, Voss T. Atlas of the human brain. Elsevier Inc, 2008

70- Maks CB, Butson CR, Walter BL, Vitek JL, McIntyre CC. Deep brain stimulation activation volumes and their association with neurophysiological mapping and therapeutic outcomes. **J Neurol Neurosurgery Psychiatry 80(6):**659-66, 2009

71- Mallet L, Schüpbach M, N'Diaye K, et al. Stimulation of subterritories of the subthalamic nucleus reveals its role in the integration of the emotional and motor aspects of behavior. **Proc Natl Acad Sci U S A 104(25):**10661-6, 2007

72- Mangin J-F. Entropy minimization for automatic correction of intensity non uniformity. Hilton Head Island, SC:IEEE Press, 162-169, 2000

73- Mattis S. Dementia Rating Scale. Professional Manual. Odessa. FL: Psychological Assessment Resources, 1988

74- Medtronic. MRI guidelines for medtronic deep brain stimulation systems, 2006

75- Mehri M, Lalys F, Maumet C, Haegelen C, Jannin P. Analysis of electrodes placement and deformations in deep brain stimulation. **SPIE Medical Imaging** 8316-32, 2012

76- Merola A, Zibettu M, Angrisano S, Rizzi L, Lanotte M, Lopiano L. Comparison of subthalamic nucleus deep brain stimulation and duodopa in the treatment of adavanced Parkinson's disease. **Mov Disord 26(4)**:664-70, 2011

77- Neelin P. The MINC file format:from bytes to brains. **Neuroimage 7(4):**786, 1998

78- Nelson HE. A modified card sorting test sensitive to frontal lobe defects. **Cortex 12:**313–24, 1976

79- Nowinski WL, Belov D, Benabid AL. An algorithm for rapid calculation of a probabilistic functional atlas of subcortical structures from electrophysiological data collected during functional neurosurgery procedures. **Neuroimage 18:**143-55, 2003

80- Nowinski WL, Belov D, Pollak P, Banabid AL. Statistical analysis of 168 bilateral subthalamic nucleus implantations by means of the probabilistic functional atlas. **Neurosurgery 57(4):**319-30, 2005

81- Nowinski WL, Thirunavuukarasuu A, Liu J, Benabid AL. Correlation between the anatomical and functional human subthalamic nucleus. **Stereotact Funct Neurosurg 85:**88-93, 2007

82- Nyul LG, Udupa JK, Saha PK. Incorporating a measure of local scale in voxel-based 3-D image registration. **IEEE Trans Med Imaging 22:**228-37, 2003

83- Obeso JA, Rodriguez-Oroz MC, Benitez-Temion B, et al. Functional organization of the basal ganglia: therapeutic implications for Parkinson's disease. **Mov Disord 23(3)**:S548-S59, 2008

84- Pallavaram S, D'Haese PF, Kao C, Yu H, Remple M, Neimat J, Konrad P, Dawant B. A new method for creating electrophysiological maps for DBS surgery and their application to surgical guidance. **Med Image Comput Comput Assist Interv 11:**670-7, 2008

85- Pallavaram S, Dawant BM, Remple M, Neimat JS, Kao C, Konrad PE, D'Haese PF. Effect of brain shift on the creation of functional atlases for deep brain stimulation surgery. **Int J Comp Assist Radiol Surg 5(3):** 221-8, 2009

86- Parent A, Hazrati LN. Functional anatomy of the basal ganglia. I. The cortico-basal ganglia-thalamo-cortical loop. **Brain Res Rev 20:**91-127, 1995

87- Parent A, Hazrati LN. Functional anatomy of the basal ganglia. II. The place of subthalamic nucleus and external pallidum in basal ganglia circuitry. **Brain Res Rev 20:**128-54, 1995

88- Parsons TD, Rogers SA, Braayen AJ, Woods SP, Troster AI. Cognitive sequelae of subthalamic nucleus deep brain stimulation in Parkinson's disease: a meta-analysis. **Lancet Neurol 5:**578-88, 2006

89- Patenaude B, Smith SM, Kennedy DN, Jenkinson M. A Bayesian model of shape and appearance for subcortical brain segmentation. **Neuroimage 56:**907-22, 2011

90- Pollo C, Vingerhoets F, Pralong E, Ghika J, Maeder P, Meuli R, Thiran JP, Villemure JG. Localisation of electrodes in the subthalamic nucleus on magnetic resonance imaging. J. **Neurosurgery 106:**36-44, 2007

91- Rodriguez-Oroz MC, Rodriguez M, Guridi J, Mewes K, Chockkman V, Vitek J, DeLong MR, Obeso JA. The subthalamic nucleus in parkinson's disease: somatotopic organization and physiological. **Brain 124(9):**1777-90, 2001

92- Reitan RM. Validity of the Trail Making test as an indicator of organic brain damage. **Percept Mot Skills 8:**271-6, 1958

93- Romanelli P, Esposito V, Schall DW, Heit G. Somatotpy in the basal ganglia: experimental and clinical evidence for segregated sensorimotor channels. **Brain Res Rev 48:**112-8, 2005

94- Rouaud T, Dondaine T, Drapier S, Haegelen C, Lallement F, Péron J, Raoul S, Sauleau P, Vérin M. Pallidal stimulation in advanced Parkinson's patients with contraindications for subthalamic stimulation. **Mov Disord 25:**1839-46, 2010

95- Saint-Cyr JA, Trépanier LL, Kumar R, Lozano AM, Lang AE. Neuropsychological consequences of chronic stimulation of the subthalamic nucleus in Parkinson's disease. **Brain 123:**2091-108, 2000

96- Saint-Cyr JA, Hoque T, Pereira LC, Dostrovsky JO, Hutchison WD, Mikulis DJ, Abosch A, Sime E, Lang AE, Lozano AM. Localization of clinically effective stimulating electrodes in the human subthalamic nucleus on magnetic resonance imaging. **J Neurosurgery 97(5):**1152 66, 2002

97- Schaltenbrand G, Wahren W. Atlas for Stereotaxy of the Human Brain. Thieme, Stuttgart, Germany, 1977

98- Schwab RS, England AC. Projection techniques for evaluating surgery in Parkinson's Disease. Third Symp on Parkinson's disease, Edinburgh, Scotland 152-7, 1968

99- Sled JG, Zijdenbos AP, Evans AC. A nonparametric method for automatic correction of intensity nonuniformity in MRI data. **IEEE Trans Med Imaging 17:**87-97, 1999

100- Smith SM. Fast robust automated brain extraction. **Hum Brain Mapp 17:**143-55, 1998

101- Stancanello J, Muacevic A, Sebastiano F, Modugno N, Cerveri P, Ferrigno G, Uggeri F, Romanelli P. 3T MRI evaluation of the accuracy of atlas-based subthalamic nucleus identification. **Med Phys 35(7):**3069-77, 2008

102- Stroop JR. Studies of interference in serial verbal reactions. **J Exp Psychology 18:**643-662, 1935

103- Talairach J, Tournoux P. Co-Planar Stereotaxic Atlas of the Human Brain. Thieme, Stuttgart, Germany, 1988

104- Temel Y, Kessels A, Tan S, Topdag A, Boon P, Visser-Vandewalle V. Behavioural changes after bilateral subthalamic stimulation in advanced Parkinson disease: a systematic review. **Parkinsonism Relat Disord 12:**265-72, 2006

105- Theodosopoulos PV, Marks WJ, Christine C, Starr PA. Locations of movement-related cells in the human subthalamic nucleus in Parkinson's disease. **Mov Disord 18(7):**791-8, 2003

106- Vayssiere N, Hemm S, Zanca M, Picot MC, Bonafe A, Cif L, Frerebeau P, Coubes P. Magnetic resonance imaging stereotactic target localization for deep brain stimulation in dystonic children. **J Neurosurg 93:**784-90, 2000

107- Volkmann J, Albanese A, Kulisevsky J, et al. Long-term effects of pallidal or subthalamic deep brain stimulation on quality of life in Parkinson's disease. **Mov Disord 24:** 1154-61, 2009

108- Weaver F, Follett K, Hur K, Ipplolito D, Stern M. Deep brain stimulation in Parkinson disease: a metaanalysis of patient outcomes. **J Neurosurg 103**: 956-67, 2005

109- Weaver F, Follett K, Stern M, et al. Bilateral deep brain stimulation vs best medical therapy for patients with advanced Parkinson disease. **JAMA 301(1)**:63-73, 2009

110- Wells WM 3rd, Viola P, Atsumi H, Nakajima S, Kikinis R. Multi-modal volume registration by maximization of mutual information. **Med Image Anal 1(1):**35-51, 1994

111- Yelnik J, Damier P, Bejjani BP, et al. Functional mapping of the human globus pallidus: contrasting effect stimulation in the internal and external pallidum in Parkinson's disease. **Neuroscience 101:**77-87, 2000

112- Yelnik J, Bardinet E, Dormont D, Malandain G, Ourselin S, Tandé D, Karachi C, Ayache N, Cornu P, Agid Y. A three-dimensional, histological and deformable atlas of the human basal ganglia. I. Atlas construction based on immunohistochemical and MRI data. **Neuroimage 37:** 618-38, 2007

113- York MK, Wilde EA, Simpson R, Jankovic J. Relationship between neuropsychological outcome and DBS surgical trajectory and electrode location. **J Neurol Sci 287:**159-71, 2009

114- Zijdenbos AP, Dawant BM, Margolin RA, Palmer AC. Morphometric analysis of white matter lesions in MR images: method and validation. **IEEE Trans Imaging 13:**716-24, 1994

Publications issues de la thèse

- Lalys F, Haegelen C, Abadie A, Jannin P. Post-operative assessment in deep brain stimulation based on multimodal images: registration workflow and validation. In Medical Imaging 2009: Visualization, Image-Guided Procedures, and Modelling

- Lalys F, Haegelen C, Ferre JC, El-Ganaoui O, Jannin P. Construction and assessment of a 3T MRI brain template. **Neuroimage 49:**345-54, 2010

- Lalys F, Haegelen C, Mehri M, Drapier S, Verin M, Jannin P. Anatomo-clinical atlases using clinical data and electrode contact coordinates: application to subthalamic deep brain stimulation. **J Neurosc Meth 212:**297-307, 2012

- Mehri M, Lalys F, Maumet C, Haegelen C, Jannin P. Analysis of electrodes placement and deformations in deep brain stimulation. **SPIE Medical Imaging** 8316-32, 2012

- Haegelen C, Coupe P, Fonov V, Guizard N, Jannin P, Morandi X, Collins DL. Automated segmentation of basal ganglia and deep brain structures in MRI of Parkinson's Disease. **Int J Comput Assist Radiol Surg 8:** 99-110, 2013

- Haegelenc, Lalys F, D'Albis T, Vérin M, Drapier S, Jannin P, Morandi X. Construction of statistical anatomo-clinical maps on medial pallidal stimulation in Parkinson's disease. **J Neurosurg** (en cours de soumission)

Communications orales

- Congrès de la Société de Neurochirurgie de Langue Française, décembre 2010, Paris, France. ***Validation de la segmentation des ganglions de la base sur un template IRM 3Tesla***. Haegelen C, Lalys F, Jannin P, Abadie A, Collins L, Brassier G, Morandi X.

- Congrès de la Société Française de Neurochirurgie, avril 2011, Dijon. ***Validation de la segmentation des ganglions de la base d'un template Parkinson*****.** Haegelen C, Fonov V, Coupe P, Lalys F, Jannin P, Morandi X, Collins DL.

Communication affichée

- Humain Brain Mapping, juin 2011, Québec, Canada. ***Validation of basal ganglia segmentation on a 3T MRI template***. Haegelen C, Guizard N, Coupé P, Lalys F, Jannin P, Morandi X, Collins DL.

Construction et validation d'une base de données multimodales pour la stimulation cérébrale profonde

Résumé en français

Introduction

La stimulation cérébrale profonde (SCP) à haute fréquence est actuellement un traitement efficace des patients ayant des mouvements anormaux. Parmi les ganglions de la base, la partie caudale du noyau ventral latéral du thalamus (VLc), le globus pallidal médial (GPm) et le noyau subthalamique (NST) sont stimulés selon la pathologie à l'origine des mouvements anormaux.

L'intervention chirurgicale de SCP comporte quatre temps opératoires. Le premier temps comporte la pose d'un cadre de stéréotaxie fixé à la tête du patient sous anesthésie locale. Le deuxième temps est la visée millimétrique de la cible sur un scanner et/ou une IRM cérébraux tridimensionnels à l'aide d'une station de planning stéréotaxique. Le troisième temps est l'implantation de l'électrode de stimulation sous anesthésie locale pour permettre l'enregistrement électrophysiologique de la cible et le testing clinique du patient par stimulation sur l'électrode. Le quatrième temps est la pose du stimulateur en sous-cutané sous anesthésie générale. Les trois premiers temps sont longs et éprouvants pour les patients, notamment à cause du sevrage brutal de leurs traitements la veille de l'intervention. L'importance de l'amélioration clinique et l'existence d'effets secondaires moteurs, neuropsychologiques voire psychiatriques en postopératoire dépendent essentiellement de la localisation anatomique de l'électrode de stimulation.

Pour améliorer la précision du ciblage, plusieurs auteurs ont construit des bases de données anatomiques, cliniques et fonctionnelles. Dans la littérature, plus la base de données est riche en informations multimodales, plus la méthode de ciblage semble précise. Dans toutes ces études, aucune donnée clinique, neuropsychologique et psychiatrique n'a été incluse. Peu d'études ont corrélées leurs résultats anatomiques aux résultats cliniques.

Le but de cette thèse est la construction d'une base de données multimodales sur la SCP pour mieux apprécier les résultats postopératoires. La première étape consiste à avoir un espace référentiel commun où tous les contacts stimulés pourront être visualisés et analysés. Pour cela, nous voulions avoir une IRM moyennée spécifique de la pathologie étudiée, la maladie de Parkinson. Sur cette IRM moyennée appelé template Parkinson, les ganglions de

la base et les structures cérébrales profondes comme l'hippocampe, ont été segmentés pour mieux les visualiser. Dans un deuxième temps, nous avons étudié 30 patients parkinsoniens stimulés dans le NST et analysé leurs résultats à partir d'atlas anatomo-cliniques. Enfin, nous avons étudié 20 patients parkinsoniens stimulés dans le GPm et analysé leurs résultats par des cartes statistiques afin d'améliorer à la fois l'analyse anatomique et clinique de ces patients.

Segmentation automatique des ganglions de la base et de structures cérébrales profondes à partir d'IRM de patients parkinsoniens

Contexte : Des techniques de segmentation cérébrale à partir de template ont été développées pour aider au ciblage des ganglions de la base en stimulation cérébrale profonde dans le cadre du traitement chirurgical des mouvements anormaux.

Objectif de l'étude : Nous avons comparé trois méthodes de segmentation cérébrale basées sur des templates pour déterminer la meilleure méthode de segmentation des ganglions de la base dans la maladie de Parkinson.

Matériels et méthodes : Nous avons d'abord construit un template IRM en séquences T1 et T2 en moyennant 57 séquences T1 avec injection de gadolinium et 42 séquences T2 réalisées chez des patients parkinsoniens. Sur ce template, 24 structures cérébrales profondes ont été segmentées manuellement et de manière bilatérale: noyau caudé, putamen, pallidum médial et latéral, NST, noyau rouge, substance noire, thalamus, corps géniculés médial et latéral, hippocampe, corps amygdaloïde. Pour valider cette segmentation, 14 des 24 structures du template ont été à nouveau manuellement segmentées sur 10 IRM de patients parkinsoniens, en choisissant des structures de tailles différentes. Nous avons ensuite comparé ces segmentations manuelles par 3 méthodes automatiques de segmentation. Deux méthodes consistaient à utiliser un outil de recalage: ANIMAL (*automatic nonlinear image matching and anatomical labeling*) développé par Louis Collins à Montréal, et SyN (*symmetric image normalization*) développé à Los Angeles. La troisième méthode était basée sur la technique de fusion à partir de patchs (*patch-based label fusion method*) développée par Pierrick Coupé à Montréal. Cette technique consistait à segmenter des structures cérébrales à partir de librairies de segmentations disponibles. Chaque voxel à segmenter était comparé à d'autres déjà segmentés sur des IRM d'anatomie comparable. Les structures obtenues automatiquement par ces trois méthodes ont été ensuite comparées à celles obtenues manuellement sur les IRM des 10 patients, en utilisant la comparaison par le taux de Dice-kappa ou coefficient de similarité. Les taux de Dice-kappa ont été comparés statistiquement selon un test de Friedman avec un seuil de significativité de 0,05.

Le centre de gravité de chaque structure a été aussi calculé selon les trois méthodes et les coordonnées des centres de gravité pour une structure donnée ont été comparées statistiquement par un test apparié de Student, avec un seuil de significativité de 0,05. Nous avons aussi estimé la variabilité interindividuelle des segmentations entre Claire Haegelen et Louis Collins en comparant les coordonnées des centres de gravité de trois structures anatomiques segmentées trois fois de suite par chaque expert: le putamen, la substance noire et le NST.

Résultats : Il n'y avait pas de différence entre les segmentations faites par les deux experts. En terme de centre de gravité, le test apparié de Student montrait une différence significative entre les segmentations automatiques obtenues par ANIMAL et la *patch-based method* (p = 0,002) et celles obtenues par SyN et la *patch-based method* (p = 0,01). Il n'y avait pas de différence entre les segmentations automatiques obtenues par ANIMAL et SyN (p = 0,13).
En ce qui concerne les résultats de taux de Dice-kappa obtenus:

- Par ANIMAL et SyN: les valeurs médianes étaient comprises entre 0,62 et 0,67 pour le NST et la substance noire, et supérieures à 0,73 pour toutes les autres structures.
- Par la *patch-based method*: les valeurs médianes étaient comprises entre 0,62 et 0,7 pour le NST et la substance noire, et supérieures à 0,76 pour toutes les autres structures.

Le test de Friedman a montré une différence significative entre les trois méthodes pour le corps amygdaloïde gauche (p = 0,014), le noyau rouge gauche (p = 0,045) et les deux thalami ($p < 0,05$).

Conclusions : Nous avons construit les premières étapes de la création d'une base de données multimodales pour la stimulation cérébrale profonde en créant un template spécifique de la maladie de Parkinson. Nous avons comparé trois méthodes de segmentation automatique des ganglions de la base et de structures profondes cérébrales pour pouvoir l'appliquer à de nouvelles données d'imagerie de patients. Même si les méthodes utilisant des outils de recalage sont les plus utilisées, la *patch-based method* a donné des résultats relativement similaires en termes de taux de Dice-kappa par rapport à ANIMAL et SyN. La *patch-based method* reste un outil ingénieur-dépendant mais serait à développer en routine clinique vu sa performance et son temps très court (10mn) pour acquérir une segmentation automatique des ganglions de la base.

Atlas anatomo-cliniques sur la stimulation subthalamique dans la maladie de Parkinson

Contexte : L'importance de l'amélioration clinique en postopératoire d'une stimulation du NST dans la maladie de Parkinson dépend essentiellement de la précision de ciblage pendant la chirurgie. Nous avons étudié les résultats moteurs de cette chirurgie et les conséquences neuropsychologiques par la création d'atlas anatomo-cliniques à l'aide d'un référentiel IRM commun dans lequel les plots stimulés ont été recalés.

Objectif de l'étude : A l'aide d'un outil statistique de fouille de données, le but était la corrélation entre la localisation des plots stimulés et les effets moteurs et neurospychologiques de la stimulation au sein d'un référentiel commun, un template IRM spécifique de la maladie de Parkinson.

Matériels et méthodes : L'étude a inclus de manière rétrospective 30 patients ayant une maladie de Parkinson et les critères habituels d'inclusion pour une stimulation du NST. Chaque patient a eu une IRM préopératoire en séquence 3D T1 avec injection de gadolinium et en séquence 3D T2, un scanner cérébral 3D préopératoire avec le cadre de Leksell et un scanner cérébral après implantation des électrodes. Les évaluations cliniques pré- et postopératoires à 3 mois incluaient le score d'UPDRS III, les échelles de Schwab et England, et de Hoehn et Yahr, ainsi que les scores neuropsychologiques usuels (MDRS, WSCT, TMT, Stroop et l'étude des fluences). La détection automatique des plots de chaque électrode a été utilisée à partir du scanner postopératoire avec une erreur de 0,96 ±0,33 mm.

Pour visualiser les plots dans un référentiel commun, nous avons comparé les erreurs de recalage obtenues avec 2 outils de recalage, Demons, développé à Rennes et SyN développé à Los Angeles, et 2 référentiels IRM, un template construit à partir de 15 IRM du même sujet (Jannin15) et le template Parkinson. Les erreurs ont été comparées statistiquement par un test de Student, avec un seuil de significativité de 0,05.

Après normalisation des scores cliniques, nous avons construit des atlas anatomo-clinques à l'aide d'un outil de Classification Hiérarchique Ascendante en limitant le nombre de groupes obtenus à deux ou trois maximum. La validation statistique de cette classification sans à priori a été faite par un test d'ANOVA.

Résultats : L'erreur de recalage était significativement plus faible avec le template Parkinson qu'avec celui Jannin15 (p = 0,025). L'erreur de recalage était aussi significativement plus faible avec l'outil SyN qu'avec Demons (p = 0,05). Nous avons donc utilisé le template Parkinson avec le recalage des patients dans ce template par SyN pour construire les atlas anatomo-cliniques. Selon les scores étudiés, nous avons obtenu les groupes suivants:

- Pour l'UPDRS III: 3 groupes de patients, le premier groupe très amélioré avec des plots en position postéro-supérieure, le deuxième groupe amélioré avec des plots en position moyenne, et un troisième groupe moins amélioré avec des plots en position inferieure du NST.
- Pour la fluence catégorielle: 2 groupes; le premier groupe avec une dégradation de la fluence avec des plots en position postérieure, et un deuxième groupe avec une amélioration avec des plots en position antérieure du NST.
- Pour la fluence lexicale: tous les patients étaient aggravés par la stimulation quelle que soit la position du plot dans le NST.
- Pour le test de Stroop: 2 groupes; un premier groupe avec une dégradation postopératoire du test de Stroop avec des plots en position antéro-inférieure, et un deuxième groupe avec une amélioration postopératoire avec des plots en position postéro-supérieure.

Pour l'analyse des autres scores moteurs et neuropsychologiques, aucun groupe n'a pu être créé par l'outil de Classification Hiérarchique Ascendante.

Conclusions : A notre connaissance, c'est la première étude à montrer que la stimulation de la région postéro-supérieure du NST a le meilleur effet moteur mais entraine une dégradation des fluences lexicale et catégorielle du fait de la localisation du plot. Par contre, les patients avaient de meilleures performances au test de Stroop dans cette même région. Ces résultats étaient concordants avec la littérature ce qui a permis de valider notre méthode de construction des atlas anatomo-cliniques. De telles données anatomo-cliniques ont pour but d'être utilisables en pratique clinique pour planifier la stimulation de nouveaux patients dans le NST.

Construction de cartes anatomo-cliniques statistiques après stimulation pallidale médiale dans la maladie de Parkinson

Contexte : Le choix entre une SCP du NST ou du GPm pour traiter des patients parkinsoniens à un stade avancé de la maladie de Parkinson est controversé dans la littérature.

Objectif de l'étude : Le but de cette étude était d'analyser les résultats moteurs et neuropsychologiques de la stimulation du GPm à l'aide d'une nouvelle méthode statistique et de données anatomiques transposées dans un référentiel commun sans à priori clinique.

Matériels et méthodes : L'étude a inclus de manière rétrospective 20 patients ayant une maladie de Parkinson et les critères habituels d'inclusion pour une SCP du GPm mais des critères d'exclusion pour une SCP du NST. Les évaluations cliniques préopératoires à 3 mois et postopératoires à 6 mois incluaient le score d'UPDRS III, les échelles de Schwab et England, et de Hoehn et Yahr, ainsi que les scores neuropsychologiques usuels (MDRS, WSCT, TMT, Stroop et l'étude des fluences). Nous avons calculé un ratio *S%* d'amélioration ou de détérioration pour chaque score par la soustraction du score postopératoire par celui préopératoire, ensuite normalisée par la soustraction du score maximum par le score minimum. Si le score s'améliorait après stimulation du GPm, le ratio *S%* devait être positif sauf pour l'UPDRS III.

Chaque patient a eu une IRM préopératoire en séquence 3D T1 avec injection de gadolinium et en séquence 3D T2, un scanner cérébral 3D préopératoire avec le cadre de Leksell et un scanner cérébral après implantation des électrodes. Chaque plot d'électrodes a été détecté automatiquement puis toutes les données anatomiques ont été recalées dans un référentiel commun, le template Parkinson. Nous avons modélisé le champ électrique autour de chaque plot stimulé selon les dernières données de la littérature, approximativement 3 mm autour de chaque plot. Ainsi une zone de stimulation couvrant plusieurs voxels sur le template Parkinson a pu être représentée par score selon une échelle de couleur figurant l'amélioration ou la détérioration du score en postopératoire. Ceci était représenté sur la carte 'Statistique'. Pour connaitre le nombre de patients représentés dans un voxel, nous avons obtenu une carte 'Patient'.

Résultats : Treize patients étaient stimulés sur un seul plot de manière bilatérale, 6 patients sur 2 plots par côté et un patient sur un plot à gauche et 2 plots à droite.
Selon l'atlas de Talairach ayant pour origine la commisssure antéreiure (CA), le plot moyen de stimulation était à 23,7 mm latéralement, 8 mm an arrière de CA, et 2,8 mm sous la ligne CA-CP. En général, les cartes 'Patients' ont montré pour tous les scores une majorité des patients stimulés en position postéro-ventrale du GPm, le coté gauche étant stimulé plus latéralement que le coté droit, soit à la limite entre le GPm et le pallidum latéral. Les cartes 'Statistiques' ont montré dans la partie postéro-ventrale du GPm:

- Pour l'UPDRS III: un ratio *S%* compris entre –0,2 et -0,12. Les patients étaient tous améliorés quelle que soit la localisation du plot stimulé.
- Pour le MDRS: un ratio *S%* compris entre 0,001 et 0,03. Les patients étaient globalement inchangés après stimulation du GPm.
- Pour la fluence catégorielle: un ratio *S%* compris entre -0,11 et 0,15. Les patients étaient soit légèrement aggravés soit améliorés.
- Pour la fluence lexicale: un ratio *S%* compris entre -0,12 et -0,05. Les patients étaient aggravés lorsque le plot stimulé était dans la partie postéro-ventrale du GPm.
- Pour le test de Stroop: un ratio *S%* compris 0,03 et 0,66. Les patients étaient globalement stables ou améliorés.

Conclusions : Nous avons donc mis au point une méthode efficace et visuelle d'appréciation du bénéfice postopératoire de la stimulation du GPm. Chez les patients parkinsoniens sévères, la stimulation du GPm les améliore du point de vue moteur sans aggravation neuropsychologique sauf du point de vue de la fluence lexicale. Les patients pouvaient même être légèrement améliorés selon le test de Stroop et la fluence catégorielle.

Les cartes 'Statistiques' et 'Patients' ont permis de visualiser la région postéro-ventrale du GPm comme étant la plus efficace pour ces patients. Notre plot moyen de stimulation était d'ailleurs plus latéral que les données de la littérature, faisant probablement intervenir la partie motrice du pallidum latéral mais en évitant la partie limbique du pallidum médial.

Conclusions

Les différentes étapes de la construction d'une base de données multimodales ont été les suivantes:

- *La construction d'un template IRM à partir de 57 patients parkinsoniens, soit un template spécifique de la maladie de Parkinson*

A partir du template parkinson, nous avons segmenté les ganglions de la base et des structures cérébrales profondes comme l'hippocampe et le corps amygdaloïde. Nous avons comparé trois méthodes de segmentation automatique pour valider la segmentation du template Parkinson. Nous avons constaté peu de différences entre ces trois méthodes en termes de précision de recalage mais par contre une différence des temps de calcul. Une nouvelle méthode appelée 'patch-based label fusion method' était la plus rapide mais nécessitait d'être appliquée par un ingénieur et non utilisable seulement par un clinicien.

- *L'utilisation de la segmentation du template Parkinson chez des patients*

Nous avons analysé les résultats de recalage de deux outils en termes de précision de recalage. Nous avons montré que l'outil le plus précis était SyN [50]. Nous avons alors recalé toutes les données anatomiques des patients sur le template Parkinson, en particulier les plots stimulés sur la segmentation des ganglions de la base. Cette étape de validation était la deuxième étape de la construction de la base de données multimodales pour pouvoir l'utiliser ensuite dans la pratique clinique afin obtenir la segmentation des ganglions de la base chez un nouveau patient.

- *L'analyse post-opératoire de 30 patients stimulés dans le NST*

Nous avons construit des atlas anatomo-cliniques à propos d'un score moteur et de quatre scores neuropsychologiques en utilisant un outil statistique non-supervisé, la Classification Hiérarchique Ascendante. Nous avons obtenu des résultats en accord avec les données de la littérature et une nouvelle explication à la dégradation constatée des fluences après une SCP du NST. Nous avons montré une discordance entre la meilleure amélioration motrice des patients stimulés dans la région postéro-supérieure du NST et

l'inévitable dégradation des fluences, induite par la stimulation de cette région. Cette troisième étape était une première approche pour corréler des données anatomiques avec celles cliniques sans à priori clinique.

- *L'analyse post-opératoire de 20 patients stimulés dans le GPm*

Pour améliorer la précédente analyse, nous avons mis au point de nouvelles cartes statistiques prenant en compte le volume de stimulation au lieu d'une représentation par un point du plot stimulé. Cette nouvelle méthode a aussi pris en compte le nombre de patients dans le volume de stimulation. Nous avons ainsi obtenu une carte 'Statistique' représentant l'évolution postopératoire du score par un code couleur, et une carte 'Patient' pour connaitre le nombre de patient dans un voxel donné. Les deux cartes étaient superposées sur la segmentation du template Parkinson. Le but était de construire des cartes utiles au neurochirurgien avant une implantation d'un nouveau patient. Nous avons démontré l'amélioration motrice des patients après stimulation du GPm sans détérioration neuropsychologique. Le plot moyen stimulé dans notre étude avait une position plus latérale dans le GPm que celui décrit dans la littérature, probablement à cause de l'atrophie cérébrale chez les patients avec une maladie de Parkinson sévère.

Ces travaux illustrent les différentes étapes de construction et de validation d'une base de données sur la stimulation cérébrale profonde afin de pouvoir l'utiliser en pratique clinique. Ceci nous a permis d'être confiants dans les étapes suivantes:

- le recalage de la segmentation du template Parkinson sur des imageries de patients, dans la limite des progrès sans cesse constants dans ce domaine;
- la visualisation des ganglions de la base sur une IRM de patient afin d'optimiser le ciblage;
- l'optimisation d'une nouvelle procédure d'implantation par l'analyse des précédents résultats postopératoires, qu'ils soient moteurs ou neuropsychologiques.

Etudes en perspective

1) Notre intention est l'utilisation en pratique clinique de la base de données selon trois étapes:

- Premièrement, une étape dite d'inclusion avec l'IRM préopératoire, comportant la segmentation automatique de la peau et du cerveau, le recalage automatique de la segmentation du template Parkinson sur l'IRM, et enfin la détection manuelle de CA et CP sur l'IRM;
- Deuxièmement, une étape dite préopératoire avec le scanner acquis le matin de l'intervention, le patient ayant le cadre stéréotaxique fixé sur la tête. Cette étape comporte la reconnaissance automatique du cadre et le recalage du scanner sur l'IRM;
- Troisièmement, une étape dite postopératoire avec le scanner postopératoire, comportant la détection automatique des plots des électrodes.

Notre but est de développer un pipeline intégré et entièrement automatique, appelé PyDBS, qui aidera au ciblage précis et à l'analyse des résultats postopératoires. Pour valider PyDBS, nous aurons besoin d'analyses prospectives d'implantation des patients, qui seront comparées à celles faites sans PyDBS. La comparaison pourra se faire en termes de résultats cliniques postopératoires et du retentissement peropératoire comme la durée de l'intervention chirurgicale. Nous espérons que cet outil raccourcisse la phase de planning préopératoire le matin de l'intervention et aussi la durée de l'intervention, aboutissant à un meilleur confort du patient.

2) Le but de créer des cartes 'Statistiques' est pour pouvoir les utiliser pour d'autres analyses comme:

- l'analyse de 10 patients ayant une maladie de Gilles de la Tourette et stimulés dans le GPm à Rennes;
- l'analyse de 40 patients avec un tremblement essentiel et/ou d'origine parkinsonienne stimulés dans le VLc.

3) Enfin, PyDBS peut être utile pour d'autres pathologies que les mouvements anormaux du fait de la segmentation de structures profondes, comme l'hippocampe et le corps amygdaloïde. Ainsi PyDBS pourrait être utilisé pour aider au ciblage du noyau antérieur du thalamus chez des patients ayant une épilepsie partielle pharmaco-résistante.

VU :

Le Directeur de Thèse Doctorale
(Nom et Prénom)

VU :

Le Responsable de l'École

VU pour autorisation de soutenance

Rennes, le

Le Président de l'Université de Rennes 1

Guy CATHELINEAU

VU après soutenance pour autorisation de publication :

Le Président de Jury,
(Nom et Prénom)

Résumé

La stimulation cérébrale profonde est un traitement efficace pour traiter les symptômes parkinsoniens chez les patients en échappement thérapeutique médical. L'intervention chirurgicale consiste à positionner au millimètre près une électrode de stimulation dans un noyau cérébral profond. La qualité du ciblage peut être améliorée par des bases de données multimodales, à la fois anatomiques, cliniques et électrophysiologiques. En premier lieu, nous avons créé une IRM moyennée appelée template Parkinson, puis nous avons validé la segmentation des 24 structures cérébrales profondes du template. Dans un deuxième temps, nous nous sommes intéressés à la meilleure localisation du plot stimulé dans le noyau subthalamique (NST) en étudiant les résultats moteur et neuropsychologiques de 30 patients parkinsoniens stimulés dans le NST. Pour chaque score clinique, nous avons obtenu un atlas anatomo-clinique, associant le degré d'amélioration ou de dégradation du patient avec son plot stimulé. Nous avons constaté une discordance entre la meilleure amélioration motrice et l'inévitable dégradation des fluences en stimulant dans la région postéro-supérieure du NST. Dans un troisième temps, nous avons développé des cartes statistiques anatomo-cliniques pour visualiser les conséquences motrices et neuropsychologiques à 6 mois d'une stimulation du pallidum médial (GPm) chez 20 patients parkinsoniens. Les patients étaient tous améliorés sur le plan moteur sans altération neuropsychologique. La zone où la majorité des patients étaient améliorés sur le plan moteur, était la partie postéro-ventrale du GPm, un peu plus latéralement que les données de la littérature. Notre but est d'utiliser les cartes statistiques de manière prospective chez d'autres patients à opérer, pour raccourcir le temps de ciblage pré-chirurgical le jour de l'intervention et pour améliorer le résultat postopératoire, tant sur le plan moteur que neuropsychologique.

Abstract

Deep brain stimulation (DBS) is an effective treatment for patients with severe disabled Parkinson's disease refractory to medical treatments. DBS surgery consists of the accurate implantation of an electrode in a deep brain nucleus. The quality of the surgical planning can be improved by developing a multimodal database based on anatomical, clinical and electrophysiologial data. The first step was to develop a specific magnetic resonance imaging (MRI) template of Parkinson's disease patients' anatomy, and to validate the segmentation of the 24 deep brain structures made on this template. Secondly, we focused on identifying optimum sites for subthalamic nucleus (STN) stimulation by studying symptomatic motor improvement along with neuropsychological side effects in 30 patients with PD. Each clinical score produced one anatomo-clinical atlas, associating the degree of improvement or worsening of the patient with its active contacts.We showed a discrepancy between a good motor improvement and an invevitable deterioration of the fluencies by targeting the postero-superior region of the STN. Finally, we developed new statistical anatomo-clinical maps the better to visualize the motor and neuropsychological consequences at 6 months of GPm stimulation in 20 patients with PD. These maps provided us with the motor improvement of GPm stimulation without cognitive impairments. We also proposed a new more lateral targeting of the GPm in PD because of the cortico-subcortical atrophy induced by the disease. Our goal is to use these statistical maps prospectively in further patients to improve their targeting, thus ensuring a shorter planning step on the day of the surgery as well as better outcomes from motor and neuropsychological point of view.